

MODE I AND MODE II INTERLAMINAR FRACTURE TOUGHNESS SIMULATION OF
UNIDIRECTIONAL AND QUASI-THREE-DIMENSIONAL COMPOSITES

By

Xinyu Mao

A THESIS

Submitted to
Michigan State University
in partial fulfillment of the requirements
for the degree of

Mechanical Engineering - Master of Science

2019

ABSTRACT

MODE I AND MODE II INTERLAMINAR FRACTURE TOUGHNESS SIMULATION OF UNIDIRECTIONAL AND QUASI-THREE-DIMENSIONAL COMPOSITES

By

Xinyu Mao

Fiber reinforced polymer (FRP) composite materials are widely used in automotive and aerospace industries. The traditional FRP composites have a laminated construction in which layers are reinforced with fibers in unidirectional (UD) or fabric forms. Such materials possess good mechanical properties in-plane but relatively weak in the through-thickness direction. Due to their low interlaminar strength, composites are prone to delamination. The quasi-three-dimensional (Q3D) composite are designed to improve the interlaminar strength. In this work, the Q3D composite is made by a special braiding process in which the bias tows are braided into adjacent layers. Contrary to the conventional composites in which plies are bonded by the polymer matrix only, the plies of Q3D composites are bridged by fiber tows. As a higher load is required to break the bridging tows for crack growth, the delamination resistance will increase. This has been proven by interlaminar fracture experiments under Mode I and Mode II conditions.

This thesis is focused on numerical simulations of UD and Q3D composites under Mode I and Mode II loadings. This investigation is needed for the development of simulation methods for crash safety simulations of Q3D composite structures in automotive applications.

In this work, the interlaminar delamination was modeled with cohesive elements. Both the Bilinear and Trilinear Cohesive Zone Models (CZM) were investigated. The CZM parameters were

determined from the Mode I and Mode II fracture toughness values measured in experiments. The simulations were performed using explicit finite element (FE) code LS-DYNA.

It was observed that in Mode I simulations, the Bilinear CZM predicted a stable crack growth, which agreed with the experimental observation. On the other hand, the Trilinear CZM predicted a relatively unstable crack growth. In Mode II experiment with an end-notched flexural (ENF) configuration, the delamination tends to be unstable. This behavior was better predicted with the Trilinear CZM.

In FE models for Q3D composite, the cohesive elements were assigned with two sets of CZM parameters. The first set of parameters was the same as that for the UD model. The second set with higher fracture toughness values was assigned to the cohesive elements corresponding to the bridging tows. This method captured the stick-slip behavior of the Q3D composites observed in Mode I experiments.

In general, the prediction was better for the UD composite than for the Q3D composite. The predicted load at the delamination initiation was within $\pm 10\%$ of the experimental values for the UD and within $\pm 15\%$ for the Q3D.

ACKNOWLEDGEMENTS

I would like to express my sincere gratitude to my advisor Dr. Xinran Xiao for her help, advice and guidance throughout my graduate research work. She not only taught me how to do research and review literature papers, but also shared her life experience with me. I learned how to become a better employee, a better master student and a better person from her. Without her guidance and help, I would be impossible for me to complete this thesis. I also want to thank Dr. and Dr. for participating in my thesis committee.

I am thankful to people who helped me throughout my research. I want to give special thanks to Shutian Yan who shared her knowledge and experience on numerical simulation with me. When I have problems on simulation, she is always willing to answer my questions and provide me a lot of valuable resources to read. I also want to thank Zhou Wu and Tony Wente who taught me a lot of experiment methods. Tony provided me with experimental data and specimen dimensions which helped me tremendously throughout my research. Lastly, I want to express my appreciation to Dr. Danielle Zeng of Ford Motor Company for her support, feedbacks and suggestions during my graduate research.

I am so grateful to my parents for providing me with the opportunity to receive great education in United States. They sacrificed a lot for me to have this opportunity studying abroad. I appreciate my friends: Chenyu Mao, Ran Bi, Haozhen Lyu for appearing in my life. They always stand by my side when I am going through tough time.

TABLE OF CONTENTS

LIST OF TABLES	vii
LIST OF FIGURES	viii
Chapter 1. Introduction	1
1.1 Fiber-Reinforced Composite Materials.....	2
1.1.1 Characteristics of Composite	2
1.1.2 Failure of Composite.....	3
1.2 Quasi-3D Composite Material	4
1.2.1 Characteristics of Q3D Composite	4
1.2.2 Manufacturing of Q3D Composite	5
1.3 Scopes of Work.....	7
1.4 Scopes of Thesis	7
Chapter 2. Literature Review	9
2.1 Interlaminar Fracture Toughness Simulation Methods.....	9
2.2 Cohesive Damage Models	9
2.3 Simulation of Z-pinned and Stitched Composites	12
Chapter 3. LS-DYNA Simulation.....	13
3.1 Numerical Model Setup	14
3.1.1 Model Dimensions and Structures for Mode I.....	14
3.1.2 Model Dimensions and Structures for Mode II	17
3.2 Cohesive Zone Law	19
3.2.1 MAT_138 Bilinear Cohesive Zone Law.....	19
3.2.2 MAT_185 Trilinear Cohesive Zone Law	25
3.3 Material Properties.....	28
Chapter 4. Simulation Results and Discussion	31
4.1 Mode I Results	31
4.1.1 UD Composite with Bilinear CZM.....	31
4.1.2 UD Composite with Trilinear CZM.....	37
4.1.3 Q3D Composite	41
4.2 Mode II Results.....	43
4.2.1 UD Composite with Bilinear CZM.....	43
4.2.2 UD Composite with Trilinear CZM.....	45
4.2.3 Q3D Composite	48

Chapter 5. CONCLUSION	50
5.1 Summary and Conclusion	50
5.2 Future Work	54
APPENDIX	55
BIBLIOGRAPHY	57

LIST OF TABLES

Table 3.1 Dimensions of Mode I DCB model	16
Table 3.2 Dimensions of Mode II ENF model	18
Table 3.3 Mode I fracture toughness values measured in DCB experiments [6]	22
Table 3.4 Mode II fracture toughness values measured in ENF experiments [6]	22
Table 3.5 Fracture toughness values of UD composite in Mode I and II	23
Table 3.6 Fracture toughness values of Q3D composite for Mode I	23
Table 3.7 Fracture toughness values of Q3D composite for Mode II	24
Table 3.8 Scaled Length parameters for UD composites in DCB and ENF simulations	26
Table 3.9 Scaled Length parameters for Q3D composites in ENF simulation	26
Table 3.10 Carbon fiber properties	29
Table 3.11 SC-15 Epoxy properties	29
Table 3.12 Composite mechanical properties	29
Table 5.1 Comparison of the predicted and measured peak load with Bilinear CZM	52
Table 5.2 Comparison of the predicted and measured peak load with Trilinear CZM	52
Table 5.3 Comparison of the predicted and measured displacement at the peak load with Bilinear CZM	53
Table 5.4 Comparison of the predicted and measured displacement at the peak load with Trilinear CZM	53
Table A.1 Different Cohesive Zone laws	56

LIST OF FIGURES

Figure 1.1 Fiber-Reinforced Composite Materials [8]	2
Figure 1.2 (a) Front-top view of Q3D composite (b) Cross-section view of Q3D composite	5
Figure 1.3 (a) Completed Q3D carbon fiber preform (b) Schematic of VARTM process [13]....	6
Figure 2.1 Schematic of DCZM [29]	11
Figure 2.2 load-displacement curve of stitch elements [33]	11
Figure 3.1 Numerical Model setup of UD Composite	14
Figure 3.2 (a) Interface of tested Q3D composite laminate (b) Cohesive layer interface of Q3D composite laminate	15
Figure 3.3 Front view of Mode II ENF model setup	17
Figure 3.4 Cohesive layer setup of Q3D composite laminate for Mode II	18
Figure 3.5 (a) MAT_138 Bilinear Traction-separation curve (b) MAT_185 Trilinear Traction-separation curve	19
Figure 3.6 Displacement in cohesive element	20
Figure 3.7 Integration points on a cohesive element	20
Figure 3.8 Architecture of the Q3D composite specimen for DCB and ENF tests [6]	28
Figure 4.1 Comparison of the experimental load-extension responses of UD DCB specimen under Mode I with the prediction with thick cohesive element with a Bilinear CZM law	31
Figure 4.2 Comparison of the experimental load-extension responses of UD DCB specimen under Mode I with the prediction with thin cohesive element with a Bilinear CZM law	32
Figure 4.3 Comparison of Bilinear CZM law with the same G_{IC} but different traction values	33
Figure 4.4 Comparison of the load-extension curves by simulations with the two CZMs	33
Figure 4.5 The experimental R curves for UD composites	35
Figure 4.6 Mode I Experiment picture of UD composite laminate	35
Figure 4.7 Comparison of Bilinear CZM with initial G_I and Bilinear CZM with average G_{IC}	36

Figure 4.8 Load-extension curve of Trilinear CZM with thick cohesive layer	37
Figure 4.9 Load-extension curve of Trilinear CZM with thin cohesive layer	38
Figure 4.10 Comparison of traction-separation curves for Bilinear CZM and Trilinear CZM	39
Figure 4.11 Load-extension curve comparison of Bilinear CZM and Trilinear CZM	39
Figure 4.12 Cohesive element deletion of Bilinear CZM	40
Figure 4.13 Cohesive element deletion of Trilinear CZM	40
Figure 4.14 Load-Extension curve of Q3D composite laminate with thick cohesive layer	41
Figure 4.15 Load-Extension curve of Q3D composite laminate with thin cohesive layer	42
Figure 4.16 Comparison of the ENF experimental Load-deflection curve of UD composite with simulation using the Bilinear CZM	43
Figure 4.17 CZM comparison with different stiffness	44
Figure 4.18 Load-deflection curve comparison with two CZMs	44
Figure 4.19 Comparison of ENF experimental Load-deflection curve with simulation with a Trilinear CZM	45
Figure 4.20 Traction-separation curves comparison for Bilinear and Trilinear CZMs	46
Figure 4.21 Load-extension curves comparison for Bilinear and Trilinear CZMs	46
Figure 4.22 Load-extension curve of Bilinear CZM for Mode II	47
Figure 4.23 Load-extension curve of Trilinear CZM for Mode II	48

Chapter 1. Introduction

Fiber reinforced polymer (FRP) composite materials have been widely used in automotive and aerospace industries since 1960s. Compared with conventional metallic materials, composites have a relatively high specific strength, specific stiffness and fatigue resistance [1]. Implementing composite materials in vehicle structures can lead to significant improvement in fuel efficiency and better acceleration. FRP composites have been used widely in the chassis and body of supercars and racing cars.

FRPs have relatively strong in-plane strength. However, the through-thickness direction strength of these materials is relatively low. The most common failure mode in FRPs is delamination. Out-of-plane impact could cause invisible damage to composites which results in delamination failure in the through-thickness direction.

To improve the interlaminar fracture toughness of a composite, methods of z-pinning and stitching [2-5] in the through-thickness direction are developed. This improvement is usually measured by interlaminar fracture toughness tests under the Mode I and Mode II conditions. In Mode I and II fracture toughness tests, z-pinning and stitching methods show better interlaminar fracture toughness strength. However, the degradation of composite in-plane strength is also observed in experiments.

To improve the interlaminar delamination resistance and remedy the in-plane property degradation, Quasi three-dimensional (Q3D) composites have been developed which uses a special triaxial braiding technique to insert bias tows into adjacent layers. Each ply is connected by bias tows

throughout the thickness of composite. Wentz et al. [6] and Zhou [7] found that Q3D composites significantly improve interlaminar fracture toughness in the through-thickness direction of composites with small in-plane property degradation.

The objective of this work is to develop a numerical simulation method to model the delamination behavior of Q3D composites. The use of cohesive element to model the delamination behavior is investigated. Two cohesive laws, i.e. the Bilinear Cohesive Zone Law and Trilinear Cohesive Zone Law, are compared. The results of this work will be useful in the development of simulation method for crashworthiness simulations of Q3D automotive structures.

1.1 Fiber-Reinforced Composite Materials

1.1.1 Characteristics of Composite

Composite materials consist of fiber and matrix. Figure 1.1 demonstrates the schematics of fiber-reinforced composite material. Different types of fibers, such as glass fiber and carbon fiber, have different material properties. Matrix can be picked from various types of materials such as polymer, metal and ceramics [8]. Diverse combinations of fiber and matrix result in unique composite material properties. Lamina that is made of fibers and matrix can become composite laminate by

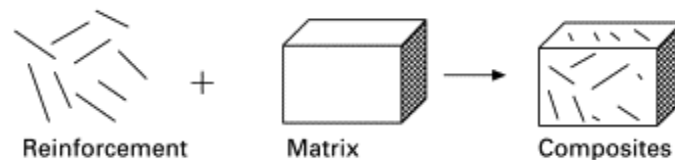


Figure 1.1 Fiber-Reinforced Composite Materials [8]

overlapping each other. The fiber preforms may be manufactured by various ways such as unidirectional, stitching, woven, braiding, etc. Each pattern gives special composite characteristics. Various orientations of laminas when stacking to compose laminate, also develop unique material properties after the composite is fabricated.

1.1.2 Failure of Composite

Composite components of airplanes and automobiles frequently undergo cyclical load that can cause degradation of the composite structure. To prevent catastrophic failure, it is critical to study the failure mode of composites [9].

Failure modes of composite laminates can be categorized by fiber failure, matrix failure, delamination failure and other types of failure. Composite fiber failure occurs when the composite is subjected to tension and compression in the direction of the fiber. Tensile load in the fiber direction could cause fiber breakage inside the composite. A crack can propagate in the matrix which can lead to matrix failure. Under compressive load, the common failure modes are fiber kinking and buckling. Another common matrix failure is due to shear. Composites have relatively weak out of plane strength compared with conventional isotropic materials. Composite material has a low ability to absorb kinetic energy applied in an out-of-plane direction [10]. Impact on a composite could create matrix damage inside the composite laminate. The crack occurs and propagates along the interface of the composite laminate eventually resulting in delamination of the laminate.

1.2 Quasi-3D Composite Material

Conventional composite lamina is made by embedding either unidirectional, 2D bi-axial, or even 2D triaxial fiber preform in epoxy. Although these fiber patterns provide relatively strong in-plane strength in the fiber direction, the delamination resistance in its out-of-plane direction become the biggest weakness. The objective of developing Q3D composite is to improve the interlaminar strength by inserting bias tows into adjacent layer to create fiber bridging between adjacent layers of laminates. Instead of having multiple layers of unidirectional or 2D woven lamina stacking on each other, Q3D laminate integrates each lamina to a uniform three-dimensional woven preform. Unlike conventional weaving technique, Q3D preforms has fiber laying down in three axes directions [11].

1.2.1 Characteristics of Q3D Composite

The failure modes of composite materials are highly depending on interlaminar integration of laminates. Q3D composites improve the interlaminar integration by attaching adjacent plies with fiber tows. Although the in-plane properties of Q3D are slightly lower than unidirectional (UD) and 2D woven composites, the delamination resistance improves significantly compared with UD and 2D woven configurations. The reinforcement in the through-thickness direction helps composite laminate absorbing more specific energy due to impact [12]. The residual strength is higher than UD and 2D woven composites after impact-induced damage. When Q3D composites are under compressive load, buckling failure appears rather than shear failure [1]. Wente et al [6] indicates that Q3D composites have higher fracture toughness than UD and 2D woven composite laminates after initiation of the crack propagation. According to Mode I DCB test, because of fiber

bridging tows in Q3D composite laminates, it requires extra work and energy to break the fiber bridging tows in composite laminates. Mode II ENF test that done by Wente et al. [6] also shows that Q3D composites has high fracture toughness.

1.2.2 Manufacturing of Q3D Composite

The Q3D composite lamina in this thesis consists of fiber tows in three directions. These are 0° , 60° and -60° . The axial carbon fiber tow lays down in 0° direction. Based on 2D woven preform, the 60° bias tow of 2D woven preform in current layer is braided into the next adjacent layer for the Q3D composite preform. In this case, two layers of 2D woven fabric are connected by 60° bias

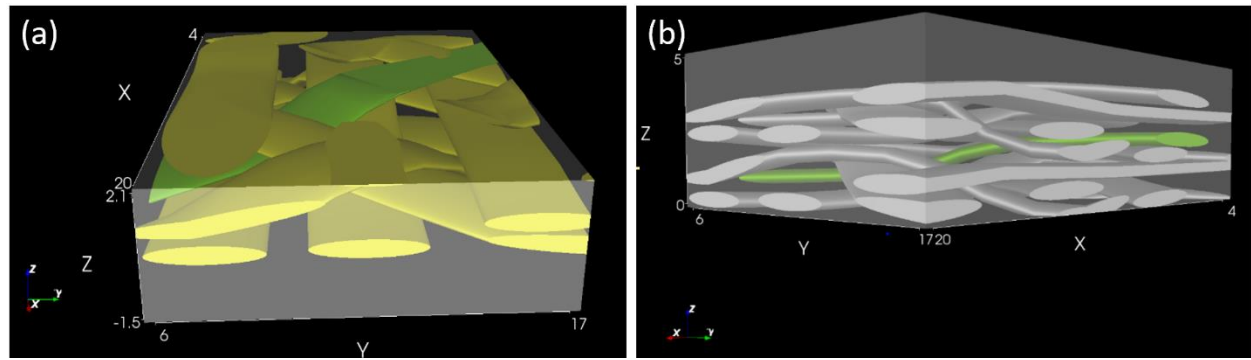


Figure 1.2 (a) Front-top view of Q3D composite (b) Cross-section view of Q3D composite

tow. Figure 1.2 shows microstructure of the Q3D composite that is created using TEXGEN. The green bias tow demonstrates inserted fiber tow which makes fiber bridging occur between adjacent lamina. The Q3D carbon fiber preform is shown in Figure 1.3 (a). Strips highlighted in red represent 0° axial tow. Yellow and green strips are 60° bridging bias tow and -60° bias tow.

The Q3D composite is manufactured by vacuum assisted resin transfer molding (VARTM) method. VARTM is commonly used by industry to manufacture large size and low volume parts. VARTM process utilizes vacuum to guide resin flow through the fiber preform. To ensure the good quality

of composite plates and avoid occurrence of voids, perfect vacuum condition inside the vacuum bag is crucial [13]. Figure 1.3 (b) demonstrates the schematic of VARTM process. Q3D preform

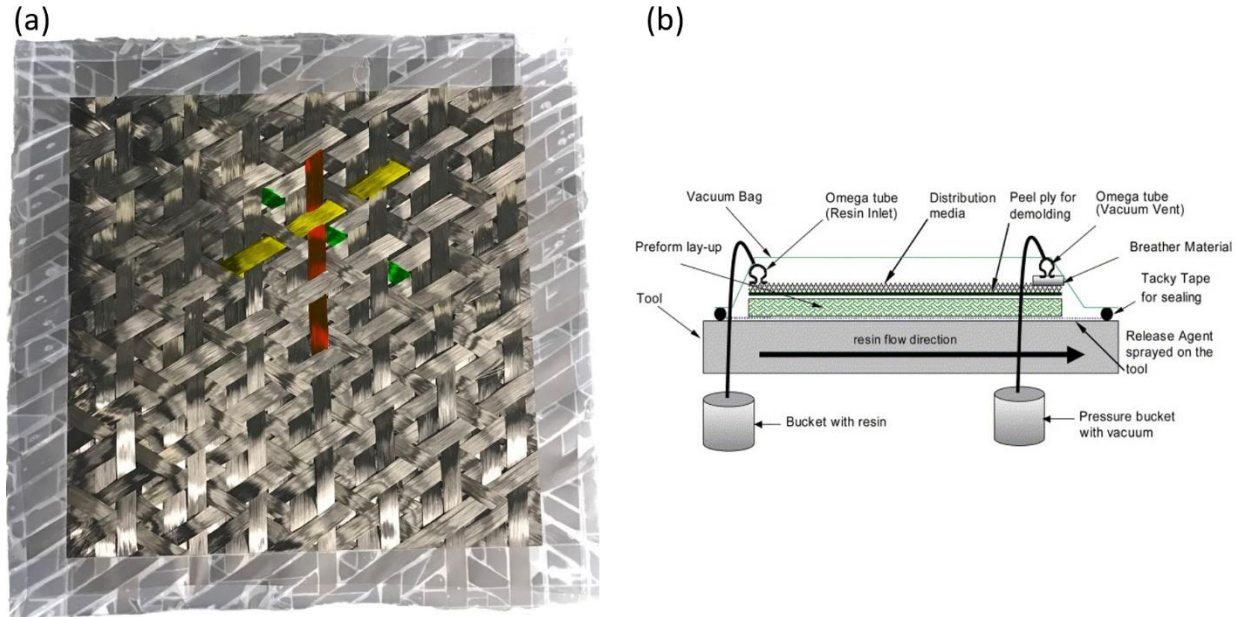


Figure 1.3 (a) Completed Q3D carbon fiber preform (b) Schematic of VARTM process [13]

that is made up of 12K, A-42 carbon fiber from DowAksa is placed on an aluminum base plate. The matrix, that is used to manufacture Q3D composite, is composed of SC-15A resin and SC-15B hardener with mix ratio of 10:3. Transfer media (distribution media), which helps resin fully impregnate with carbon fiber preform, is placed on top of the peel ply. The peel ply, which is inserted between the transfer media and composite preform, provide easy demolding after curing. Vacuum bag seals on top of the distribution media. Pressure bucket with vacuum assist pulls the resin from left to right of the Omega tube. After curing for 8 hours in auto-clave, the Q3D composite plate is manufactured.

1.3 Scopes of Work

The importance of studying the interlaminar strength of composite materials is well recognized. To prevent catastrophic structural failure of composites in the through-thickness direction, studying interlaminar strength, especially delamination behavior, of composites is significant. The improvement of the delamination resistance in the out-of-plane direction of Q3D composites is proved by experiment. Testing the performance of composite materials is relatively challenging. To manufacture perfect composite specimens requires a lot of practice. For the sake of saving time and cost on conducting experiments, it is more efficient to numerically predict system of failure beyond elastic region of laminated composite materials. Commercial finite element softwares such as LS-DYNA, ABAQUS, ANSYS are developed to predict failure mode, post-failure behavior of composite materials. The numerical simulation incorporates composite material properties (young's modulus, density, poisson's ratio in each direction of the material), which can be obtained experimentally, into composite models. The objective of this research is using finite element method to simulate interlaminar fracture toughness tests and investigate the delamination resistance of Q3D composites. LS-DYNA software is used in this research to build a FE model to simulate Mode I DCB and Mode II ENF tests of Q3D composite materials using bilinear and trilinear cohesive zone models. The load-extension curve is compared with experimental results to check prediction accuracy.

1.4 Scopes of Thesis

In this thesis, numerical models are developed using bilinear and trilinear cohesive zone models to represent delamination resistance of Q3D composite laminates under Mode I and Mode II

conditions. The input parameters of numerical models are obtained from experiments [15] and literature papers [14].

This thesis is organized as follows:

Chapter 1 introduces the general characteristics and failure modes of fiber-reinforced composite materials. The Quasi-3D composite is introduced in this chapter.

Chapter 2 provides literature review on numerical method of simulating interlaminar fracture toughness tests. The cohesive zone models in literature paper are studied and summarized in this chapter.

Chapter 3 describes LS-DYNA simulation work. The numerical model setups and dimensions are provided for both Mode I and Mode II simulations. The governing equations and cohesive laws for cohesive zone models are presented. The material and mechanical properties of the composite that is used in the simulation are shown in this chapter.

Chapter 4 The results of Mode I and Mode II simulations using bilinear and trilinear cohesive zone model are presented. The load-extension curves of simulation are compared and discussed with experimental results. The initial and average interlaminar fracture toughness values are used to investigate their influences on the prediction results. The effects on prediction results of using two different definitions of shell thickness reference plane are also investigated.

Chapter 5 concludes and summarizes the findings in this research. The future work and improvements are suggested.

Chapter 2. Literature Review

2.1 Interlaminar Fracture Toughness Simulation Methods

The fiber-reinforced composites have low interlaminar strength in the through-thickness direction. One of the common failure modes of fiber-reinforced composite laminates is delamination. There are two common approaches to numerically predict the delamination in composite laminates. Linear Elastic Fracture Mechanics (LEFM) is one of the methods to simulate the delamination behavior. Liu and Zou et al. [15-16] demonstrated that LEFM, particularly the Virtual Crack Closure Technique (VCCT) [16-19], can be used to model the delamination crack growth with an initial crack. The downside of this approach is that it is time-consuming and difficult to complete the calculation of fracture parameters such as energy release rate for progressive crack growth. Another approach is to use damage mechanics. Cohesive Zone Method (CZM) belongs to this approach. It is simpler to implement CZM in finite element models than VCCT.

2.2 Cohesive Damage Models

In CZM method, different traction-separation laws have been developed to study the fracture process of various materials [20-22]. These CZM laws have been employed in delamination modeling of composite materials.

Jung et al. [23] built an intralaminar damage model using continuum damage mechanics [24] and interlaminar damage model using cohesive zone method for glass fiber-reinforced polypropylene (GFPP) composites. The mix mode bending (MMB) test was simulated using LS-DYNA. The bilinear traction separation law [25] was used in CZM. Liljedahl et al. [26] also used a bilinear

traction-separation law in CZM to model adhesively bonded joints. The CZM model was inserted between two adjacent shell layers. The results show that the CZM damage model using a bilinear traction-separation law successfully predicted the experiment results of MMB test. Turon et al. [27] also used cohesive elements to simulate the Mode I DCB test of the unidirectional carbon fiber-reinforced composite. Turon et al. [27] compared CZM simulation results of using different interface strength values with analytical solution LEFM. The simulation results show good agreement with the LEFM solution. It was also mentioned that the penalty stiffness, the fracture toughness for Mode I and Mode II, the mixed mode interaction parameter and the interface strength are important parameters for cohesive damage model to accurately predict delamination. Turon et al. [27] simulated the Mode II ENF test using cohesive elements and plane stress elements in the through-thickness direction to predict the delamination behavior of the UD carbon fiber-reinforced composite laminate. The pre-damage cohesive elements were inserted in the pre-crack area to prevent the penetration of crack interfaces. The results were well-agreed with the analytical solution (LEFM) despite the use of different interface strength values.

In addition to CZM, decohesive elements and discrete cohesive zone model (DCZM) have also been developed to simulate interlaminar fracture toughness tests of composites. A numerical model has been developed with decohesive elements that has zero-thickness. Camanho et al. [28] developed the decohesive model which could predict the crack initiation and propagation of composite laminates under mixed mode loading. The Mode I and Mode II interlaminar fracture

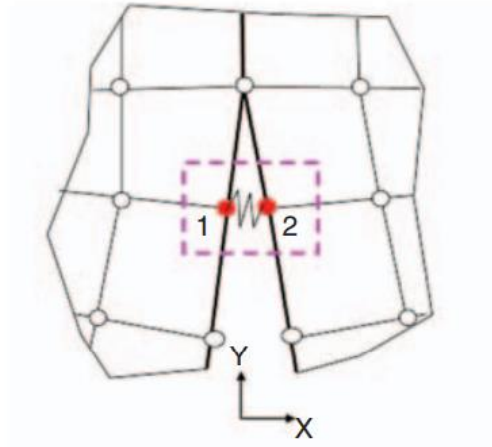


Figure 2.1 Schematic of DCZM [42]

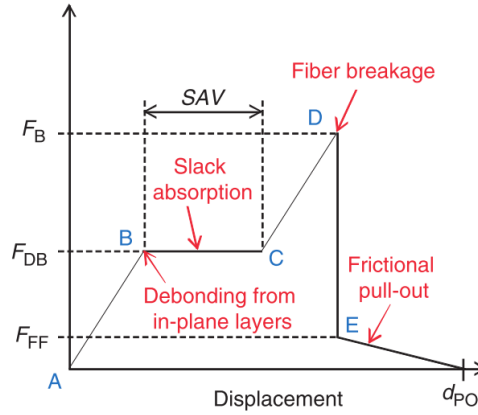


Figure 2.2 load-displacement curve of stitch elements [40]

toughness tests were simulated using decohesive cohesive model by Camanho et al. at [28]. The results show good consistency with experimental results. The discrete cohesive zone model (DCZM) was developed by treating cohesive elements as spring [29]. The schematic of DCZM is shown in Figure 2.1. The “spring” connects two nodes of adjacent elements in DCZM. In Xie’s paper [30], an improved DCZM was discussed. The strain field at the crack tip was integrated in the DCZM. The DCZM can be scaled as a function of element size. The geometric nonlinearity and crack orientation were incorporated in mode mixity of the DCZM. The Mode I simulation in [29] shows accurate prediction of the maximum load and the slope compared to test results.

2.3 Simulation of Z-pinned and Stitched Composites

To improve the interlaminar strength of composite laminates, the z-pinning method is used to increase delamination resistance. The review of z-pinned composite laminates, which was done by Mouritz [31], shows that the z-pinned composite laminates have significant improvement on delamination toughness which could resist crack propagation. Grassi and Zhang et al. [4] had used an existing micro-mechanical material model [32] to create numerical model of z-pinned composite laminate to simulate the Mode I test. A non-linear FEA was used with Newton-Raphson method to predict crack propagation. Results show that the z-pinned composite laminates have good energy absorption ability. The load drop phenomenon, which is caused by existence of fibers in the z direction, was observed in load-extension curve.

Stitching is another approach to increase interlaminar strength in composite laminates. Tan et al. [5] simulates Mode I DCB test with 2D FE model of Vectran-stitched composite laminate. In Chen et al. [33], 2D FE model had been proved to have sufficient prediction accuracy when simulating the Mode I DCB test of stitched composite laminates. The stitches in 2D FE model were created by 3-nodes rod elements. The behavior of the rod elements is governed by load-displacement curve in Figure 2.2. The stitch fracture process has four procedures: interfacial debonding, slack absorption, fiber breakage and pullout friction. Integrating all of procedures into FE model results in accurate numerical prediction. [33]

Chapter 3. LS-DYNA Simulation

In this research, the finite element model is created using LS-DYNA software. LS-DYNA is a commercial finite element program. Its explicit solver is widely used in automotive and aerospace industries in crash safety simulations. The numerical model of UD and Q3D composites are built for simulating Mode I double cantilever beam (DCB) test and Mode II end-notched flexure (ENF) test. The fracture toughness parameters for UD and Q3D models are obtained from Wentz et al. [6]. Other input parameters for material model are estimated based on the Robert et al [14]. The load-extension curve of simulation is compared with experimental results for validation of the numerical models.

The FE model for the DCB and ENF specimens were built for the unidirectional (UD) composite laminate first. The UD composite laminate has 12 layers with 0° fiber direction. Shell elements are used to model composite plies. To simulate delamination resistance of UD composite laminates, cohesive elements are utilized with bilinear and trilinear cohesive zone laws. Results are compared with experimental results to pick optimal cohesive zone law for Mode I and Mode II.

The FE model for Q3D composite material is based on the model for the unidirectional (UD) composite laminate. To simulate Q3D composite laminates, the interface of tested Q3D specimens are examined to identify the area of fiber bridging tows. The fiber bridging tows increase the delamination resistance in Q3D composites. The region enclosed by red lines in Figure 3.2 (a) is where fiber bridging appears. For fiber bridging area, higher fracture toughness values are used to simulate higher delamination resistance due to fiber bridging.

3.1 Numerical Model Setup

3.1.1 Model Dimensions and Structures for Mode I

To compare the simulation results with the experimental results of Mode I interlaminar fracture toughness test, the dimensions of the specimen and its boundary conditions in numerical model must be consistent with the specimen in experiment. The dimensions of the specimen were selected according to ASTM D5528 [34], as listed in Table 3.1. The pre-crack was manually created by inserting a Teflon film of 25-micron thickness in the mid-plane of the composite laminate when the composite plate was manufactured.

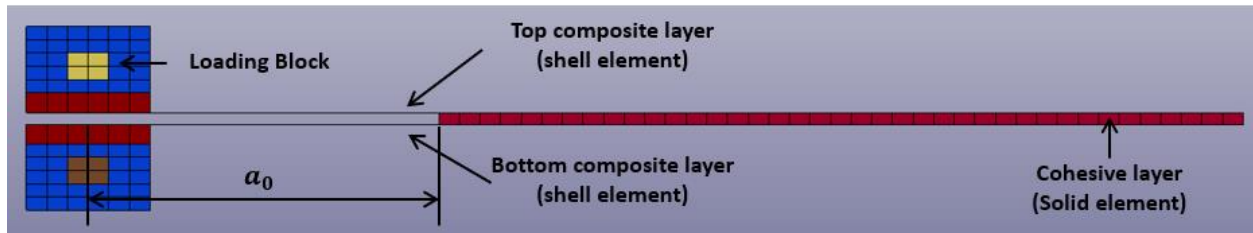


Figure 3.1 Numerical Model setup of UD Composite

The UD composite laminate has 12 layers with fiber directions in 0° , 60° and -60° . Figure 3.1 shows the numerical model setup for the Mode I simulation. The DCB model consists of the top and bottom composite layers and the interface is represented by a layer of cohesive elements.

The top and bottom composite layers are modeled using shell elements. The reasons of using shell elements are: 1. The components of automobiles and airplanes are often made of thin sheets of metals or composite materials. It is quite common to use shell element in crash safety simulation, particularly in automotive application. 2. Crash simulation are solved by explicit method. In this method, the solution accuracy is controlled by the timestep, which is in turn determined by the

smallest element size. If solid elements are used to model composite layers, the resulted timestep will be small. So that the run time to solve the problem will be long. Using shell elements will save computational time.

The shell element for composite layer is 1.8 mm thick, with 6 integration points through the thickness. Each integration point represents one ply of composite laminates. The interface where the interlaminar delamination to occur is modeled using solid cohesive elements (Figure 3.1). The cohesive layer thickness is depending on the definition of shell reference plane. In the first case, when shell thickness reference is defined at the mid-plane, the cohesive layer thickness equals to the shell thickness which is 1.8 mm. In the second case, the shell thickness reference is defined at the top surface for bottom composite layer and at the bottom for top composite layer. Then the cohesive layer thickness can be reduced to 0.336 mm. The region without cohesive elements is the pre-crack area. The loading blocks, which are modeled using solid elements with rigid material properties, are placed at the tip of the laminate. A prescribed displacement is assigned at the center

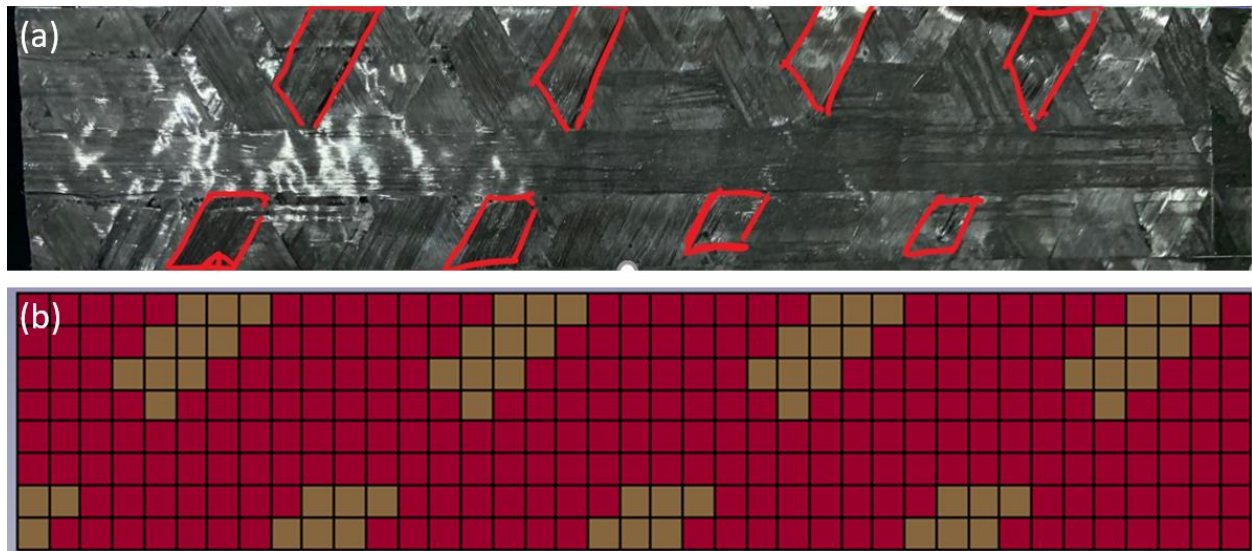


Figure 3.2 (a) Interface of tested Q3D composite laminate (b) Cohesive layer interface of Q3D composite laminate

of the top loading block with strain rate of 0.04 mm/s. The top loading block is constrained to allow only translational degree of freedom in the z direction and rotational DOF in the x direction. The bottom loading block is fixed except the rotation about the x-axis.

For the Q3D composite laminates, the structure of numerical model is identical to the UD composite laminates. The dimensions of the Q3D model is listed in Table 3.1. A unique feature of the Q3D composite laminate is the bias bridging tow which connects adjacent layers of the composite laminate. Figure 3.2 (a) shows a post-modern DCB specimen where the bias tow bridging areas are enclosed by red lines. Two sets of Cohesive Zone Model (CZM) parameters are used in the model. The elements in red had the same CZM parameters as in the UD model. The brown cohesive elements representing the 60° bias bridging in Figure 3.2(b) were assigned with a second set of CZM parameters with a higher fracture toughness value. In simulations, the brown cohesive elements produced a higher delamination resistance for laminate interface. It required larger traction force to separate the top and bottom composite layers.

Table 3.1 Dimensions of Mode I DCB model

	Length (mm)	Width (mm)	Thickness (mm)	Pre-crack (mm)
UD	184.375	25.4	3.6	52.125
Q3D	182.924	25.4	3.6	60.013

3.1.2 Model Dimensions and Structures for Mode II

The ENF specimen for Mode II experiment follows ASTM D7905 [35]. The composite laminate is placed on two bottom supporters with 4-inch span. The distance from bottom right supporter to the end of the pre-crack (a_0) is 30 mm. The upper roller in Figure 3.3 is placed above the composite laminate. The UD composite laminate dimensions are shown in Table 3.2. It consists of top and bottom composite layers. The cohesive layer is located between the top and bottom composite layers. Six pairs of automatic surface to surface contacts are defined. The contact surface of the shell element is placed at a distance equal to half of the contact thickness. The default contact

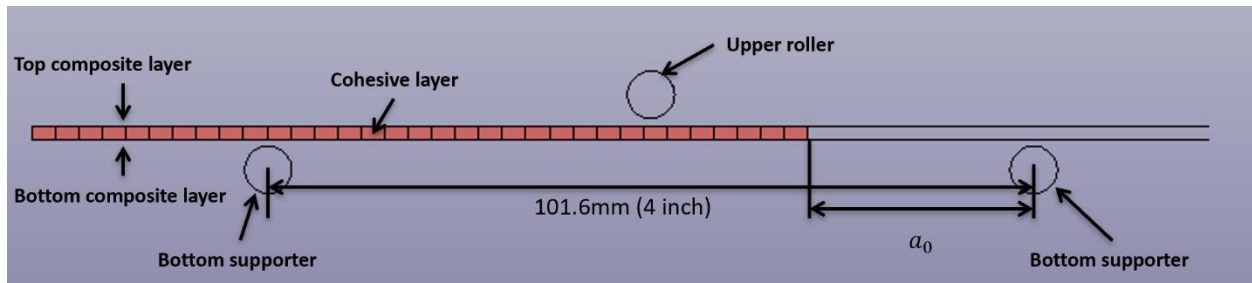


Figure 3.3 Front view of Mode II ENF model setup

thickness equals the shell thickness which is 1.8 mm [36]. The shell thickness reference plane is defined at the middle in Mode II numerical model. So that the contact surface is at the mid-plane between top and bottom composite layers. If the shell thickness reference is defined at the bottom for top composite layer and at the top for bottom composite layer, the contact surface will have initial penetration. In LS-DYNA contact cards, the master and slave selections are not necessarily following the contact sequence [37]. The optional thickness for the master and slave surface (MST, SST) are the true element thickness of the contact components. In this model, the true thickness of the shell composite layer is 1.8 mm. The cohesive layer true thickness is zero. The Rayleigh

damping coefficient for composite layer is set to be 0.05. The strain rate of Mode II ENF simulation is 0.005 mm/s.

Table 3.2 Dimensions of Mode II ENF model

	Length (mm)	Width (mm)	Thickness (mm)	Pre-crack (mm)
UD	156.25	20	3.6	53.125
Q3D	143.75	20	3.6	53.125

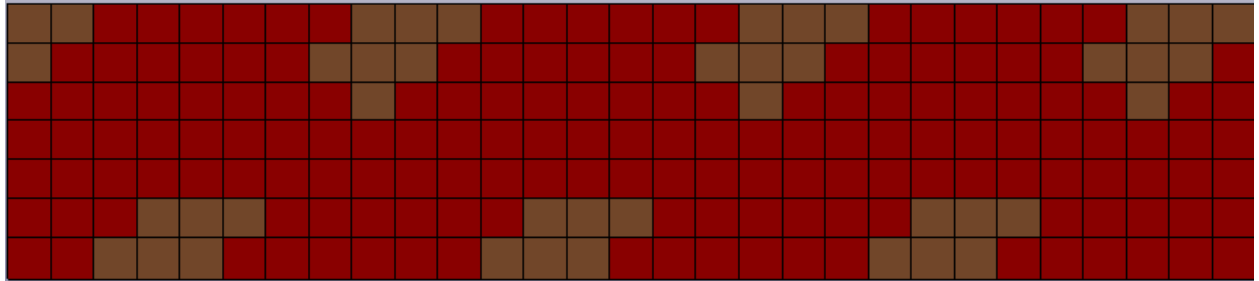


Figure 3.4 Cohesive layer setup of Q3D composite laminate for Mode II

The dimensions of the Q3D composite laminate are listed in Table 3.2. Two sets of CZM parameters are used. The cohesive layer setup is shown in Figure 3.4. A set of CZM parameters with higher fracture toughness values is assigned to brown cohesive elements to simulate higher delamination resistance of bias bridging tows.

3.2 Cohesive Zone Law

There are four typical traction-separation laws to govern the behavior of cohesive elements. Table A.1 demonstrates the traction-separation curves for different material cards in LS-DYNA. In this research, two CZM laws, i.e. MAT_138 and MAT_185 are used to simulate Mode I and Mode II interlaminar fracture toughness tests.

3.2.1 MAT_138 Bilinear Cohesive Zone Law

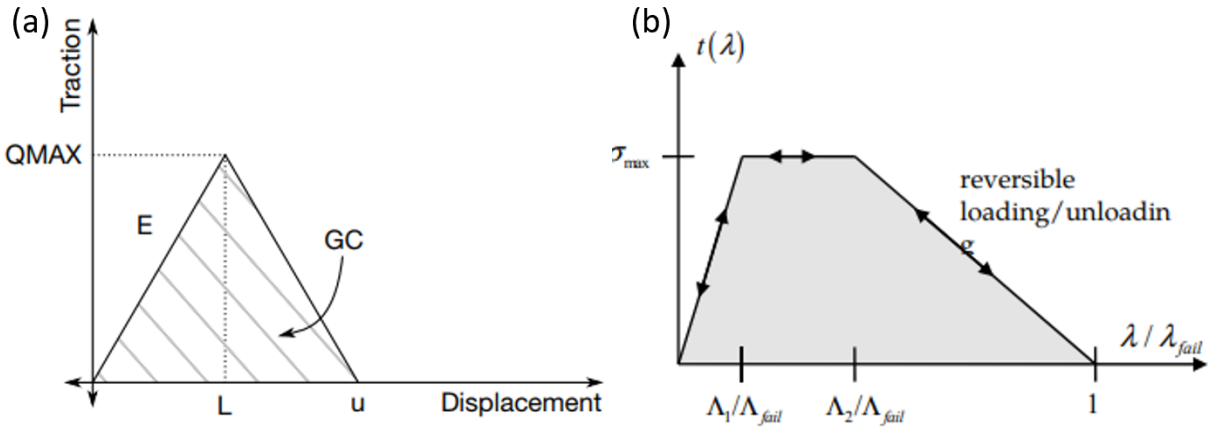


Figure 3.5 (a) MAT_138 Bilinear Traction-separation curve (b) MAT_185 Trilinear Traction-separation curve [25]

MAT_138 in LS-DYNA is governed by a bilinear traction-separation law with quadratic mixed mode delamination criterion and damage formulation to simulate delamination behavior of cohesive elements. In order to use MAT_138, cohesive element formulation 20 is defined in SECTION_SOLID of cohesive elements [25]. The 8-nodes cohesive element is used to generate cohesive layer. The number of integration points for a cohesive element to be deleted is set to 4. The tractions are defined as middle point between each pair of nodes (1-5, 2-6, 3-7, 4-8) on an 8-

nodes cohesive element in Figure 3.7. [25] A cohesive element will be deleted if 4 integration points of the cohesive element reach their peak traction.

The Bilinear Cohesive Zone Law complies mixed mode criterion [12]. The total mixed mode displacement (δ) is governed by Eq 3.1:

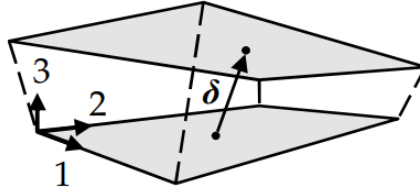


Figure 3.6 Displacement in cohesive element

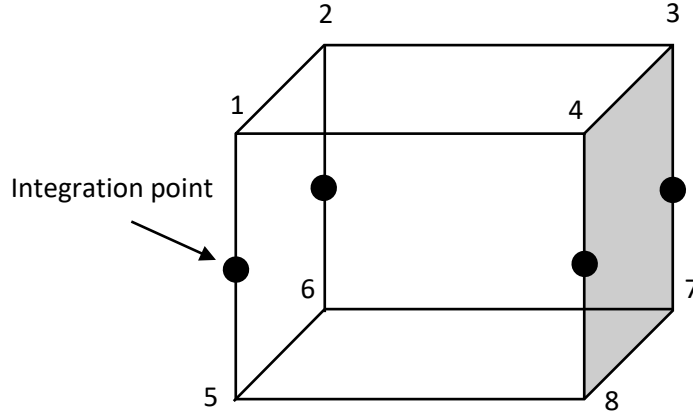


Figure 3.7 Integration points on a cohesive element

$$\delta = \sqrt{(\delta_1)^2 + (\delta_2)^2 + (\delta_3)^2} \quad (3.1)$$

Figure 3.6 illustrates the displacement inside the single cohesive element. The displacement in 3 direction (δ_3) represents the displacement in normal direction for mode I. The displacement in 1 (δ_1) and 2 (δ_2) directions are the displacement in tangential direction for mode II. The damage initiation displacement for mode I (δ_I^0) is calculated by dividing peak traction in normal direction

(T) by normal to cohesive element stiffness (EN). For mode II damage initiation displacement (δ_{II}^0) is obtained by dividing peak traction in tangential direction (S) by in-plane stiffness of cohesive element (ET). The damage initiation displacement is shown in Eq 3.2:

$$\delta^0 = \delta_I^0 \delta_{II}^0 \sqrt{\frac{1+\beta^2}{(\delta_{II}^0)^2 + (\beta \delta_I^0)^2}} \quad (3.2)$$

Where $\beta = \frac{\delta_{II}}{\delta_I}$. The total failure mixed-mode displacement is provided in Eq 3.3, where the mixed mode criterion exponential (XMU) is set to be 1.

$$\delta^F = \frac{2(1+\beta^2)}{\delta^0} \left[\left(\frac{EN}{G_{IC}} \right)^{XMU} + \left(\frac{ET \times \beta^2}{G_{IIC}} \right)^{XMU} \right]^{-\frac{1}{XMU}} \quad (3.3)$$

Figure 3.5 (a) provides the traction-separation curve for the bilinear cohesive zone law. The area under the triangle represents the energy release rate which is also known as the fracture toughness G_{IC} for mode I, and G_{IIC} for mode II. The traction within the cohesive elements increases as the separation of cohesive elements increases until reaching peak traction. The softening process starts after the peak load is reached. Eventually the traction drops to zero when failure of cohesive elements occurs.

The experimentally measured mode I and mode II fracture toughness values (G_{IC}, G_{IIC}) for UD and Q3D composites by Wentz et al. [6] are listed in Table 3.3 and Table 3.4. The parameters in the CZM laws were determined using the average fracture toughness for Mode I and non-pre-crack (NPC) fracture toughness values for Mode II. These values are listed in Table 3.5.

For Q3D, a second set of CZM parameters with higher Mode I and II fracture toughness values were introduced to model the bridging bias tows. Since the DCB and ENF specimens had different width, the area ratio of the bridging tows on the fractured specimens were different. Therefore, the second set CZM parameters were slightly different for the DCB and ENF specimens. For the DCB specimen, the volume fraction of bias tows is 19.55% which calculated using Eq 3.4. The volume

Table 3.3 Mode I fracture toughness values measured in DCB experiments [6]

	UD	2DW	Q3D
$G_{IC} [\frac{J}{m^2}]$	563.6	564.1	466.3
$G_{IC} [\frac{J}{m^2}]$	732.8	730.4	884.7
Energy [J]	3.345	3.756	4.994

Table 3.4 Mode II fracture toughness values measured in ENF experiments [6]

	UD	2DW	Q3D
NPC	644.5	502.2	613.8
PC	559.5	696.1	824.3

fraction of matrix (V_{matrix}) is 80.45%. The average Mode I fracture toughness value of Q3D composite laminates that measured in experiment ($G_{IC_{Q3D}}$) is $8.847 \times 10^{-4} GPa \cdot mm$. The Mode I fracture toughness for the bias tow elements ($G_{IC_{bias\ tow\ elements}}$) can be calculated using Eq 3.5. Table 3.6 presents the fracture toughness values for DCB simulations.

In ENF simulation of Q3D composites, the width of the numerical model is shorter than the width of the Q3D model in Mode I. The volume fraction of bias tow cohesive elements is 20.7%. The Mode I fracture toughness value is then re-calculated to be $1.466 \times 10^{-3} \text{ GPa} \cdot \text{mm}$. Table 3.7 present the fracture toughness values for ENF simulations

Table 3.5 Fracture toughness values of UD composite in Mode I and II

Composite	Mode I Fracture Toughness Value $G_{IC} \text{ (GPa} \cdot \text{mm)}$	Mode II Fracture Toughness Value $G_{IIC} \text{ (GPa} \cdot \text{mm)}$
Unidirectional (UD)	7.33×10^{-4}	6.44×10^{-4}

Table 3.6 Fracture toughness values of Q3D composite for Mode I

Q3D composite	Mode I Fracture Toughness Value $G_{IC} \text{ (GPa} \cdot \text{mm)}$	Mode II Fracture Toughness Value $G_{IIC} \text{ (GPa} \cdot \text{mm)}$
Matrix cohesive elements	7.33×10^{-4}	6.14×10^{-4}
Bias tow cohesive elements	1.507×10^{-3}	8.24×10^{-4}

Table 3.7 Fracture toughness values of Q3D composite for Mode II

Q3D composite	Mode I Fracture Toughness	Mode II Fracture Toughness
	Value G_{IC} (GPa · mm)	Value G_{IIC} (GPa · mm)
Matrix cohesive elements	7.33×10^{-4}	6.14×10^{-4}
Bias tow cohesive elements	1.466×10^{-3}	8.24×10^{-4}

$$V_{bias\ tow} = \frac{\text{Number of Bias tow cohesive elements}}{\text{Total number of cohesive elements}} \quad (3.4)$$

$$G_{IC\ Q3D} = G_{IC\ bias\ tow\ elements} * V_{bias\ tow} + G_{IC\ matrix\ elements} * V_{matrix} \quad (3.5)$$

$$\frac{u}{L} = \frac{2G_{IC}}{EN\left(\frac{T}{EN}\right)^2} > 1 \quad (3.6)$$

$$\frac{u}{L} = \frac{2G_{IIC}}{ET\left(\frac{S}{ET}\right)^2} > 1 \quad (3.7)$$

The relationship between the ultimate displacement at failure (u) and displacement at the peak load (L) for the bilinear traction-separation law is shown in Eq 3.6 and Eq 3.7. The ultimate displacement at failure (u) must be larger than the displacement at peak load (L). The G_{IC} and G_{IIC}

values in Eq 3.6 and 3.7 are given, the peak tractions in the normal (T) and tangential (S) directions are estimated. The normal to cohesive element stiffness (EN) and the in-plane stiffness of cohesive element (ET) can be calculated using Eq 3.6 and 3.7. The relationship between the fracture toughness values and the peak tractions is indicated in Eq 3.8 and 3.9. The ultimate displacement in the normal direction (UND) and the ultimate displacement in the tangential direction (UTD) are calculated by using Eq 3.8 and 3.9.

$$GIC = T \times \frac{UND}{2} \quad (3.8)$$

$$GIIC = S \times \frac{UTD}{2} \quad (3.9)$$

3.2.2 MAT_185 Trilinear Cohesive Zone Law

MAT_185 in LS_DYNA follows a trilinear cohesive law. It was developed by Tvergaard and Hutchinson in 1992 [20] to use with cohesive element formulations [25]. The area under the trapezoidal traction-separation curve in Figure 3.5 (b) represents the fracture toughness value. The peak tractions in the trilinear cohesive law and the bilinear cohesive law have equivalent values. The scaled distance for failure (λ_{fail}) is 1. The scaled distance to the peak traction (λ_1) is set to 0.2 and the scaled distance to beginning of softening (λ_2) is set to 0.5. The values of λ_1 and λ_2 can be adjusted.

In DCB and ENF simulation of UD composites using Trilinear CZM, the fracture toughness parameters in the Bilinear CZM are the one used here to calculate the scaled length in the normal (NLS) and tangential directions (TLS) using Eq 3.10 and 3.11. The peak traction σ_{max} is 0.009

GPa. The NLS and TLS values for UD composites in DCB and ENF simulations are listed in Table 3.8 and Table 3.9.

$$G_{IC} = \frac{1+(\lambda_2-\lambda_1)}{2} \sigma_{max} * NLS \quad (3.10)$$

$$G_{IIC} = \frac{1+(\lambda_2-\lambda_1)}{2} \sigma_{max} * TLS \quad (3.11)$$

Table 3.8 Scaled Length parameters for UD composites in DCB and ENF simulations

Composite	Scaled Length in Normal Direction (NLS)	Scaled Length in Tangential Direction (TLS)
Unidirectional (UD)	0.1253	0.110

Table 3.9 Scaled Length parameters for Q3D composites in ENF simulation

Q3D composite	Scaled Length in Normal Direction (NLS)	Scaled Length in Tangential Direction (TLS)
Matrix cohesive elements	0.1253	0.1050
Bias tow cohesive elements	0.2506	0.1409

In ENF simulation of Q3D composites, two sets of fracture toughness parameters in the Bilinear CZM of Q3D composites are used to calculate NLS and TLS using Eq 3.10 and 3.11 for bias tow cohesive elements and matrix cohesive elements.

Looking at the cohesive element model in Figure 3.6, the dimensionless separation of the element (λ) combines the interaction between the displacement in Mode I (δ_3) and Mode II (δ_1, δ_2) in Eq 3.12. The trilinear traction-separation law used for stress calculation is show in Eq 3.13. The normal and tangential components of traction vector are given by Eq 3.14 [25].

$$\lambda = \sqrt{\left(\frac{\delta_1}{TLS}\right)^2 + \left(\frac{\delta_2}{TLS}\right)^2 + \left(\frac{\delta_3}{NLS}\right)^2} \quad (3.12)$$

$$t(\lambda) = \begin{cases} \sigma_{max} \frac{\lambda \cdot \lambda_{fail}}{\lambda_1} & \lambda < \frac{\lambda_1}{\lambda_{fail}} \\ \sigma_{max} & \frac{\lambda_1}{\lambda_{fail}} < \lambda < \frac{\lambda_2}{\lambda_{fail}} \\ \sigma_{max} \frac{1-\lambda}{1-\frac{\lambda_2}{\lambda_{fail}}} & \frac{\lambda_2}{\lambda_{fail}} < \lambda < 1 \end{cases} \quad (3.13)$$

$$\begin{bmatrix} t_1 \\ t_2 \\ t_3 \end{bmatrix} = \frac{t(\lambda)}{\lambda} \begin{bmatrix} \frac{NLS}{TLS^2} & 0 & 0 \\ 0 & \frac{NLS}{TLS^2} & 0 \\ 0 & 0 & \frac{1}{NLS} \end{bmatrix} \begin{bmatrix} \delta_1 \\ \delta_2 \\ \delta_3 \end{bmatrix} \quad (3.14)$$

3.3 Material Properties

The A-42, 12k carbon fiber, which is manufactured by DowAksa, is used to make our UD and Q3D preforms. The properties of the fiber are listed in Table 3.10. SC-15 Epoxy was used as matrix resin. The properties of SC-15 Epoxy [38] are given in Table 3.11. The composite panels for interlaminar fracture testing were made with 10 layers of commercial triaxial braided composite as the outer layers and two layers of handmade composite preform at the interface, as shown in Figure 3.8. The composites were manufactured by the VARTM process.

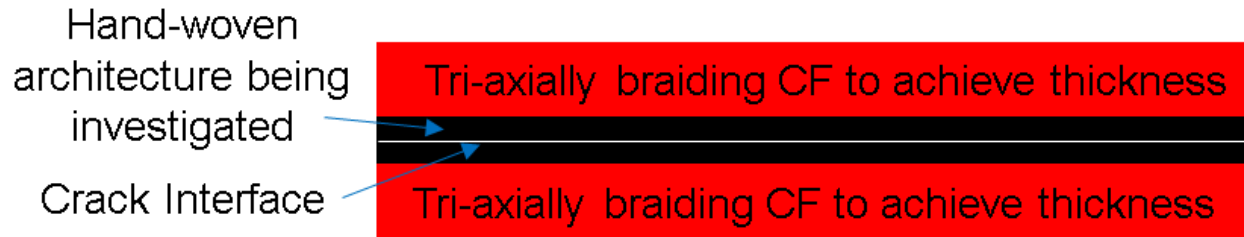


Figure 3.8 Architecture of the Q3D composite specimen for DCB and ENF tests [6]

The fiber volume fraction of the composite was estimated by acid digestion [6]. The Rule of Mixture (Eq 3.15) is then utilized to calculate composite density. The composite density is $1.46 \times 10^{-6} \text{ kg/mm}^3$. As the mechanical properties of the UD and Q3D composites are unknown, they were assumed to be close to the commercial triaxial braided composite. Literature data on T700/PR520 UD composite [14] were used to compute the properties of the triaxial braided composite using Micromechanics approach. Table 3.12 presents the estimated mechanical properties for the composite layers.

Table 3.10 Carbon fiber properties

Carbon Fiber	Tensile Strength (GPa)	Tensile Modulus (GPa)	Strain (%)	Density (g/cm ³)
A-42, 12k	4.2	240	1.8	1.78

Table 3.11 SC-15 Epoxy properties

Matrix	Density (g/cm ³)	Compressive Strength (GPa)	Viscosity (centipoises)
SC-15	1.09	0.088	300

$$\rho_{composite} = \rho_{matrix}V_{matrix} + \rho_{fiber}V_{fiber} \quad (3.15)$$

Table 3.12 Composite mechanical properties

Mechanical Properties	Unit	Carbon Fiber Composite
Density	Kg/m ³	1460
Axial modulus	GPa	38
Transverse modulus	GPa	32.7
In-plane shear modulus	GPa	8.96
In-plane Poisson's ratio	—	0.3
Axial tensile failure strain	—	0.0216
Axial compressive failure strain	—	0.018

Table 3.12 (cont'd)

Transverse tensile failure strain	—	0.0168
Transverse compressive failure strain	—	0.011
In-plane shear failure strain	—	0.024
Axial tensile stress at failure	GPa	1.044
Axial compressive stress at failure	GPa	0.377
Transverse tensile stress at failure	GPa	0.362
Transverse compressive stress at failure	GPa	0.345
In-plane shear stress at failure	GPa	0.307

4.1 Mode I Results

4.1.1 UD Composite with Bilinear CZM

Two different thicknesses of cohesive layers are investigated here. For the first case, the shell thickness reference plane is defined the middle. The cohesive layer thickness is 1.8 mm which is relatively thick compared to the second case, where the shell thickness reference plane is defined at the top for bottom shell and at the bottom for top shell and the cohesive layer is relatively thin. The load-extension curve for the unidirectional composite laminate with thick bilinear CZM is compared with the experimental load-extension curve in Figure 4.1. The green curve indicates the

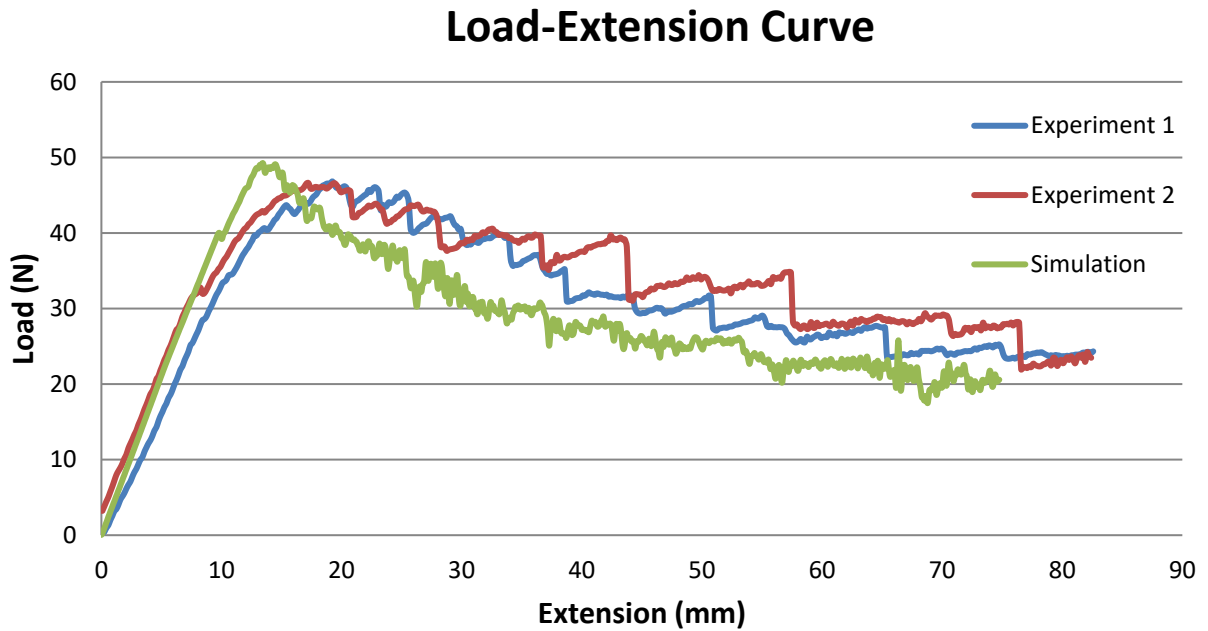


Figure 4.1 Comparison of the experimental load-extension responses of UD DCB specimen under Mode I with the prediction with thick cohesive element with a Bilinear CZM law.

simulation result and the blue and red curves illustrate the experimental result. Before load reaches its peak value, the load-extension curve generally displays a linear elastic behavior. However, the

non-linearity is also observed at approximately 12 mm. A similar trend is also observed in Beckermann's experiment [39]. The stiffness and crack growth results of the simulation agree well with the experimental load-extension curve. The numerical prediction of the peak load is higher than the experiment. After the peak load, the softening part of the load-extension curve has the same trend compared with the experimental result. The numerical simulation is unable to precisely

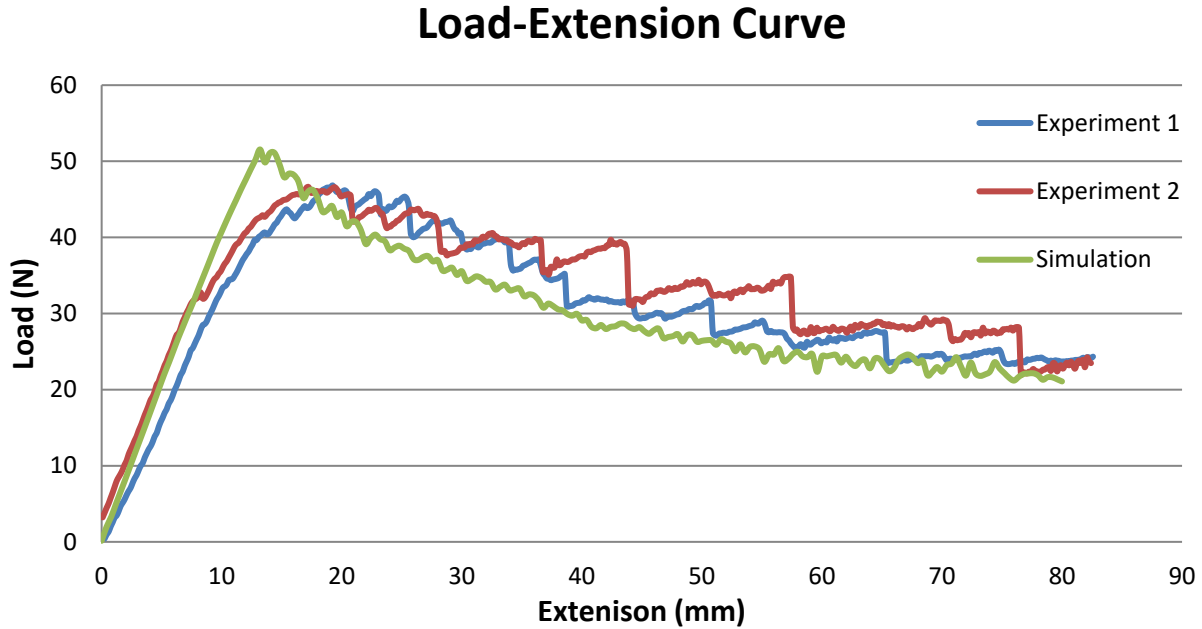


Figure 4.2 Comparison of the experimental load-extension responses of UD DCB specimen under Mode I with the prediction with thin cohesive element with a Bilinear CZM law.

predict the instability of crack propagation in the experiment due to delamination resistance of matrix [40]. The oscillation of the DCB also observed in simulation after the crack starts to propagate.

The result of thin Bilinear CZM is presented in Figure 4.2. The load-extension curve generally has the same elastic load increase to initiate the crack propagation compared with experimental results. The load decrease after the peak has the same trend as the experiment. The peak load is over-

predicted. In the simulation, the FE model with a thin cohesive layer in the DCB tends to be more stable compared with the one with a thick cohesive layer.

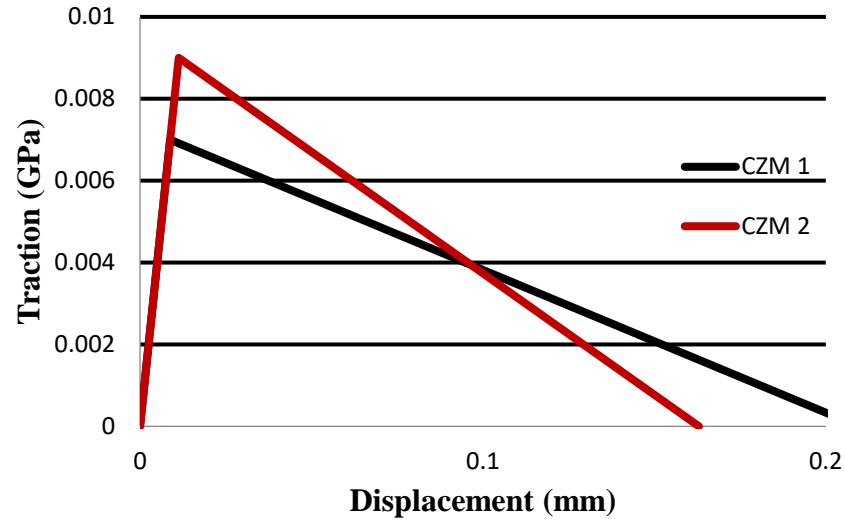


Figure 4.3 Comparison of Bilinear CZM law with the same G_{IC} but different traction values.

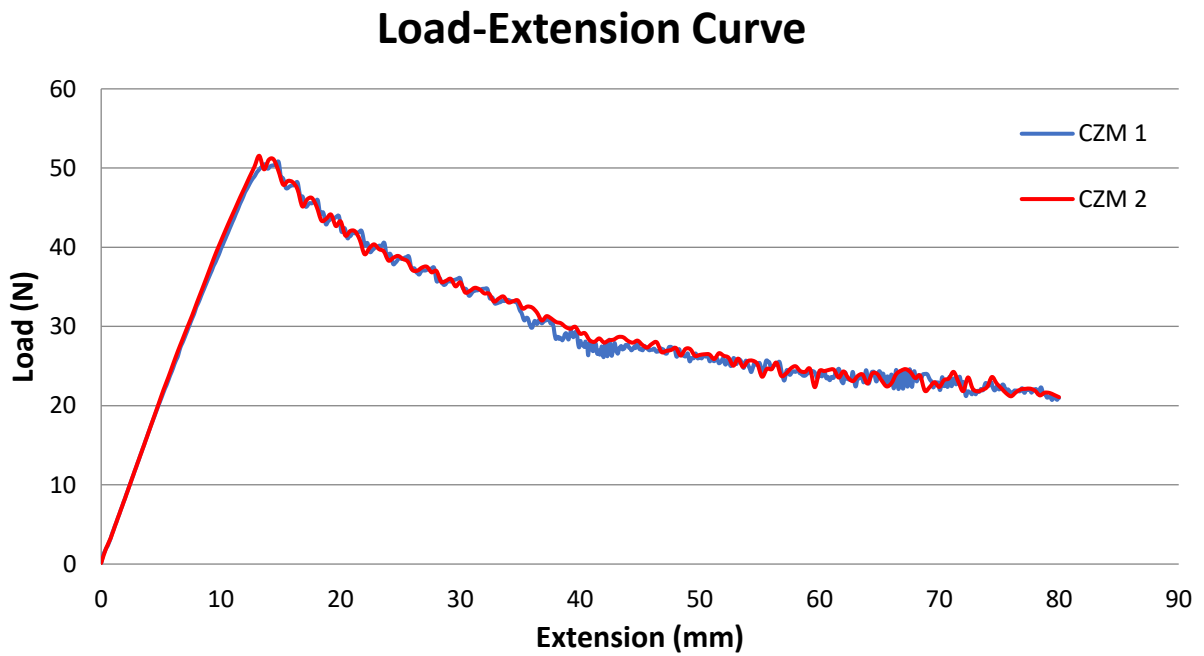


Figure 4.4 Comparison of the load-extension curves by simulations with the two CZMs

Two different bilinear traction-displacement curves are compared in Figure 4.3. The fracture toughness values that are used for Mode I simulation remain unchanged for Cohesive Zone Model 1 and 2. CZM 1 and 2 have the same linear elastic slope of the traction-displacement curve. The peak load of CZM 2 is higher than CZM 1. To keep the Mode I fracture toughness value G_{IC} unchanged for CZM 2, the ultimate displacement at failure (u) needs to be reduced for CZM 2. Figure 4.4 indicates that load-extension curves for Bilinear CZM 1 and CZM 2 are identical in stiffness, maximum load and crack growth. It is interesting to note that, if the Mode I fracture toughness value stays the same for two different bilinear traction-separation laws, the numerical predictions with two sets of CZM parameters have no major differences. It is important to use the correct Mode I fracture toughness value in the CZM in simulating interlaminar fracture toughness tests.

Eq 4.1 is used to calculate the Mode I fracture toughness value from DCB experiment, where P is the measured load in Mode I experiment, δ is the load point displacement, b is the specimen width, a is the delamination length and C is the compliance.

From the Mode I experiment, two fracture toughness values are obtained: the initial value and the averaged value. In Table 3.3, the initial fracture toughness value G_I is calculated using the measured load to initiate the crack propagation. The Figure 4.5 shows the G_{IC} values that calculated using the load before each “stick-slip” [41-42]. The average fracture toughness value G_{IC} is higher than the initial fracture toughness value G_I because the fiber bridging has occurred in the UD specimens in Mode I experiment. In Figure 4.6, fiber bridging is clearly observed in the red circle.

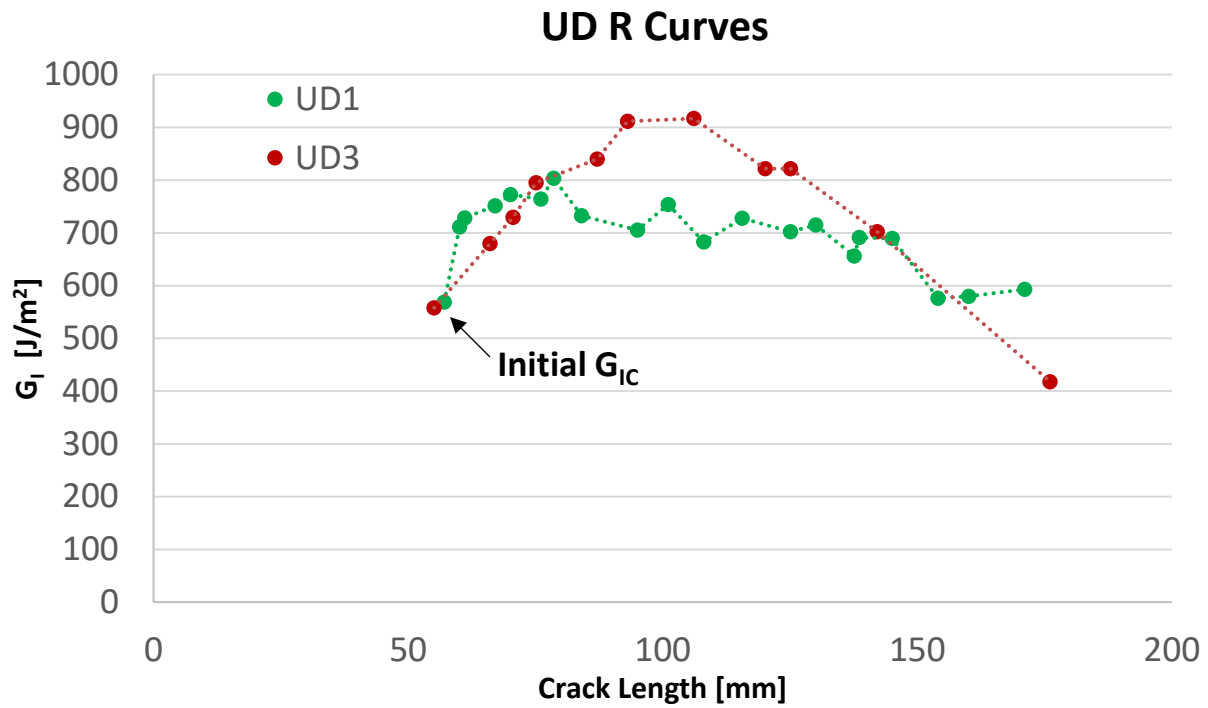


Figure 4.5 The experimental R curves for UD composites

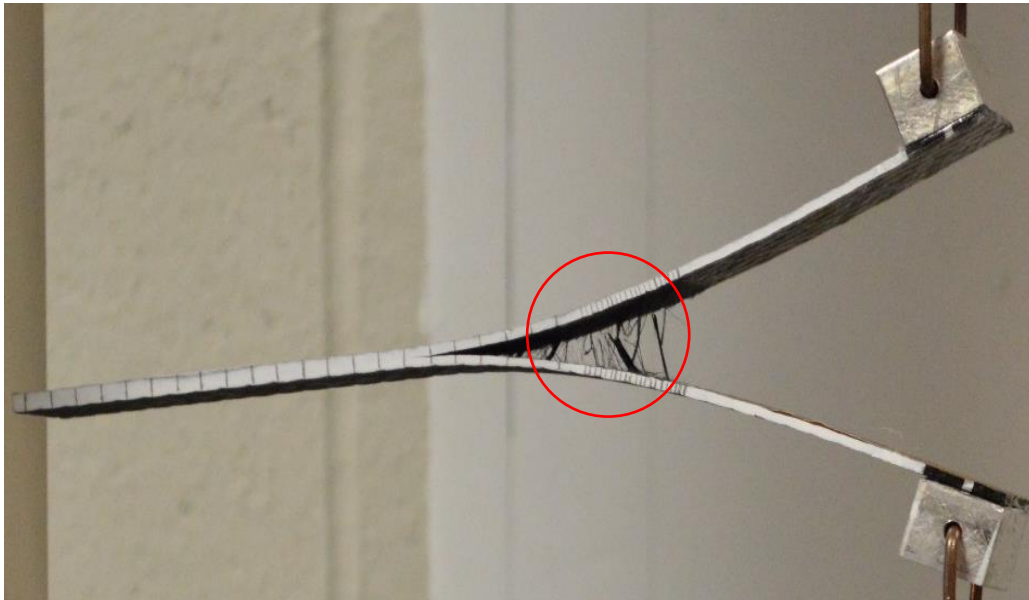


Figure 4.6 Mode I Experiment picture of UD composite laminate

$$G_{IC} = \frac{3P\delta}{2b(a+|\Delta|)} \quad (4.1)$$

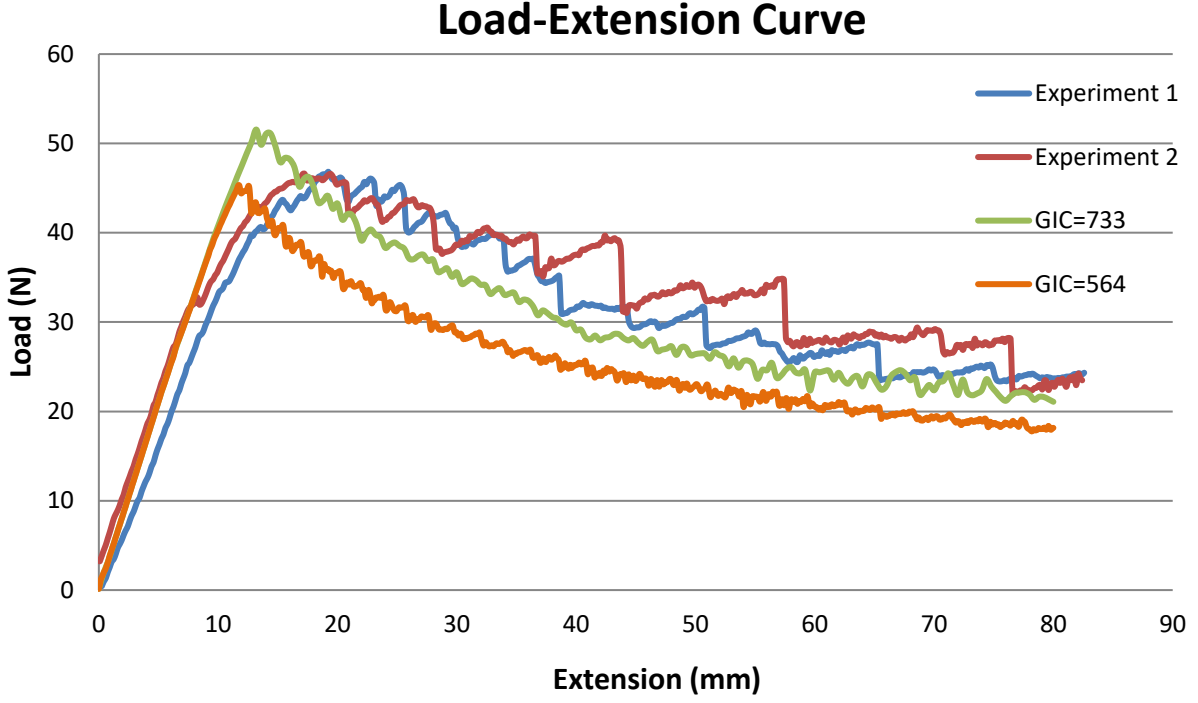


Figure 4.7 Comparison of Bilinear CZM with initial G_I and Bilinear CZM with average G_{IC}

The initial fracture toughness value G_I is used in Bilinear CZM parameters, the numerical prediction result is compared with the load-extension curve result obtained by using average fracture toughness value. Figure 4.7 shows the load-extension curve results. The green curve indicates the numerical prediction result of Bilinear CZM with the average fracture toughness value G_{IC} . The orange curve represents the prediction result of Bilinear CZM with the initial fracture toughness value G_I . The elastic and softening behavior of the load-extension curves are the same for Bilinear CZM with initial G_I and average G_{IC} . However, the numerical result of using a higher fracture toughness value gives a higher peak load prediction. The same phenomenon was observed in Turon et. al [27]. The CZM using the initial fracture toughness value G_I predicts better peak load than CZM using average fracture toughness value G_{IC} . The CZM with average fracture

toughness value G_{Ic} overshoots the peak load but has better prediction of softening behavior. To precisely predict the crack onset and propagation in UD composites under Mode I condition, incorporating both the initial and average fracture toughness values in CZMs is recommended.

4.1.2 UD Composite with Trilinear CZM

The UD DCB experiments were also simulated with a Trilinear CZM law. Thick and thin cohesive layers are also investigated with Trilinear CZM. Figure 4.8 demonstrates the load-extension curve of Trilinear CZM with thick cohesive layer. The elastic load increase to initiate the crack propagation is consistent with the experiment results. The peak load is over-predicted. The DCB tend to be unstable as the crack starts to propagate.

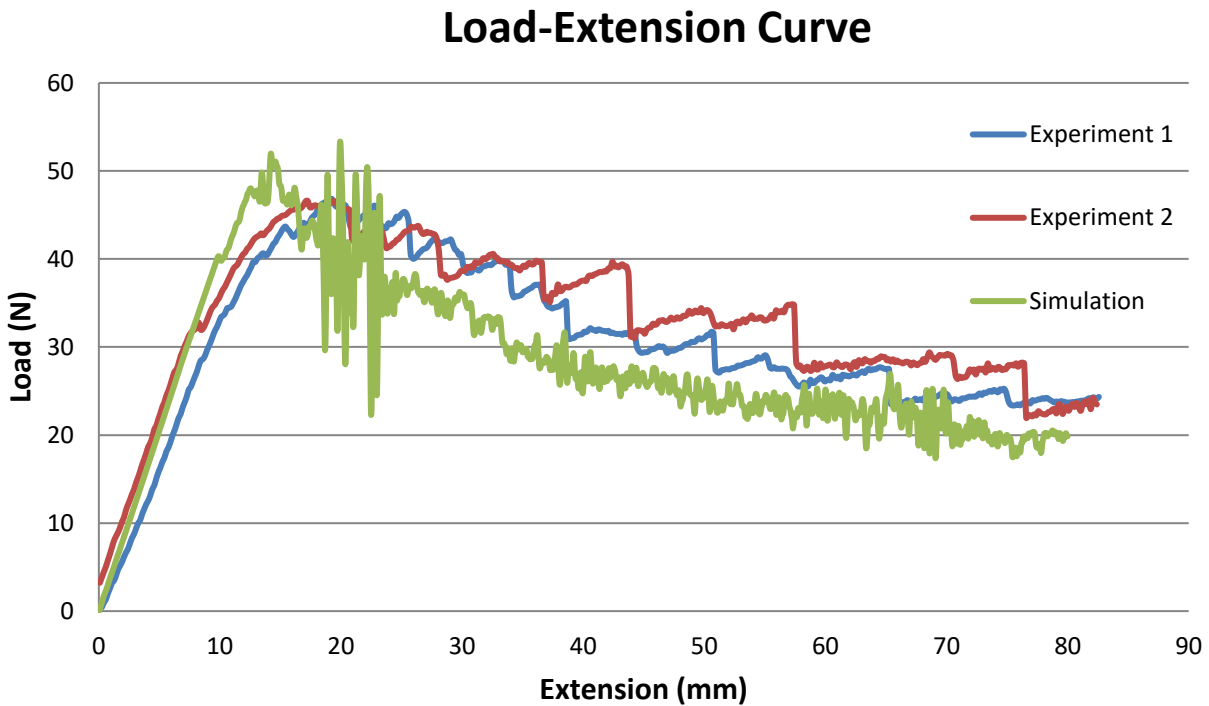


Figure 4.8 Load-extension curve of Trilinear CZM with thick cohesive layer

Looking at the load-extension curve of Trilinear CZM with thin cohesive layer in Figure 4.9, the elastic part of the load-extension curve agrees with the experiment. The peak load is over-predicted. After the peak load, the instability is observed.

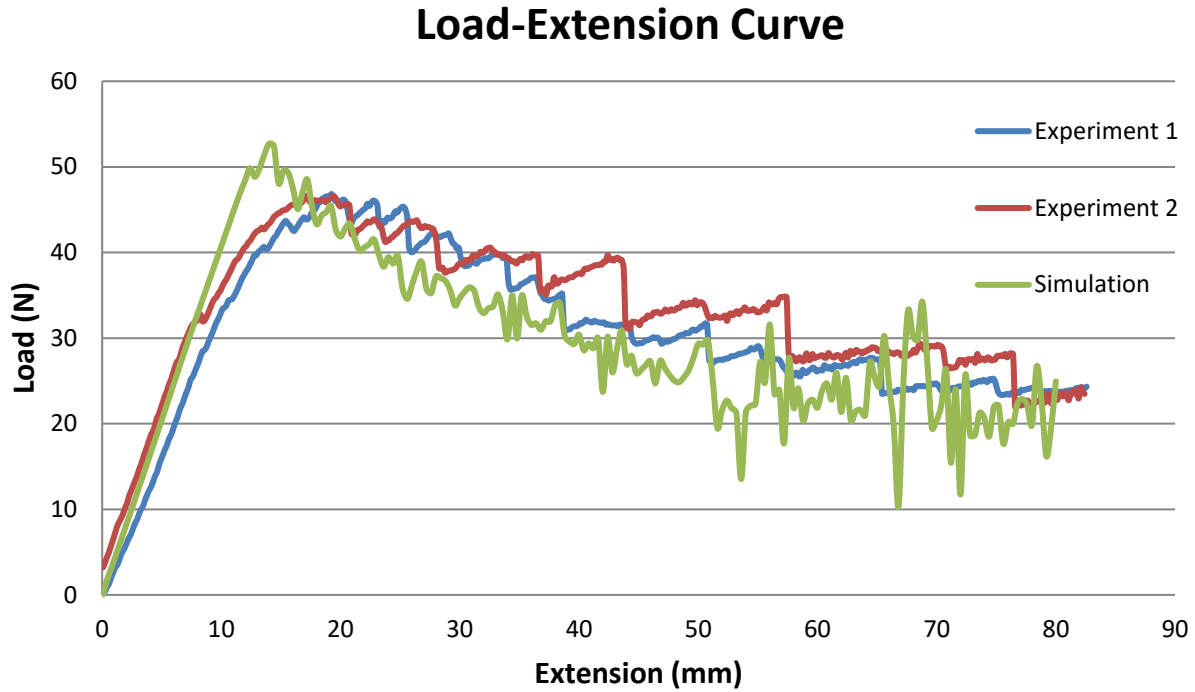


Figure 4.9 Load-extension curve of Trilinear CZM with thin cohesive layer

The traction-separation curve is compared with the Bilinear CZM law in Figure 4.10. The fracture toughness values are the same for both CZM laws. The elastic slope of traction-separation curve for the Bilinear CZM to reach the peak traction is the same as the Trilinear CZM. With the same maximum traction, Trilinear CZM has a smaller ultimate displacement at failure (u) that eventually leads to a steeper slope of the softening process. The simulation results are shown in Figure 4.11. The orange and green curves are corresponding to Bilinear and Trilinear CZMs. The elastic behavior of Trilinear CZM has the same trend as that of the Bilinear CZM. The non-linearity is not observed in load-extension curves of both Bilinear and Trilinear CZMs. The peak load of the

Trilinear CZM agrees with that of the Bilinear CZM. The instability of Trilinear CZM is observed in load-extension curve after the peak load.

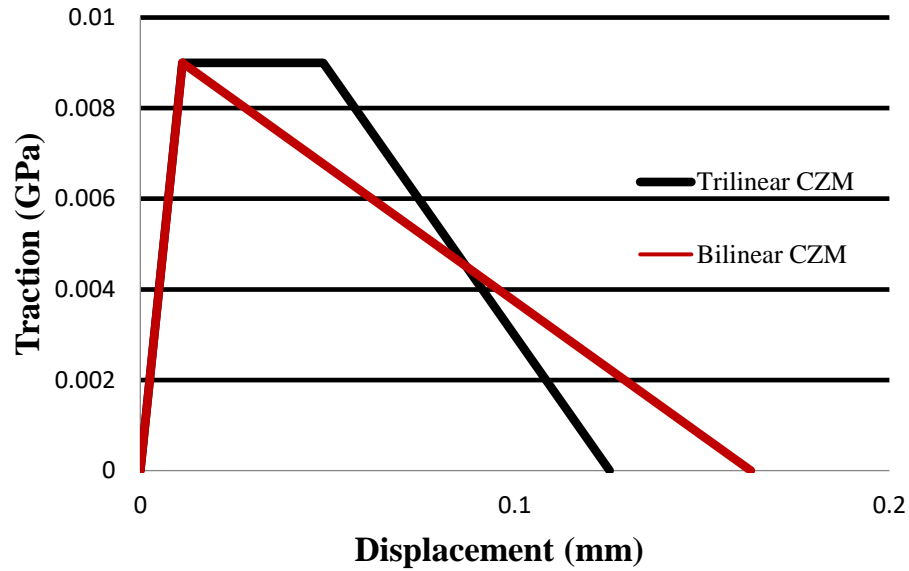


Figure 4.10 Comparison of traction-separation curves for Bilinear CZM and Trilinear CZM

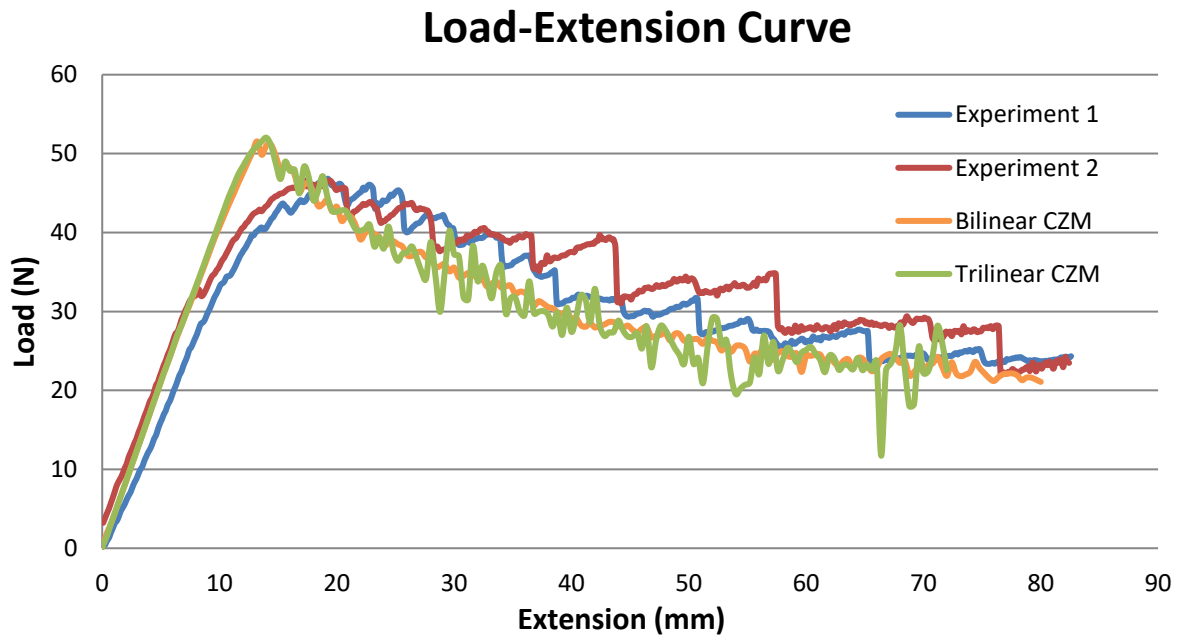


Figure 4.11 Load-extension curve comparison of Bilinear CZM and Trilinear CZM

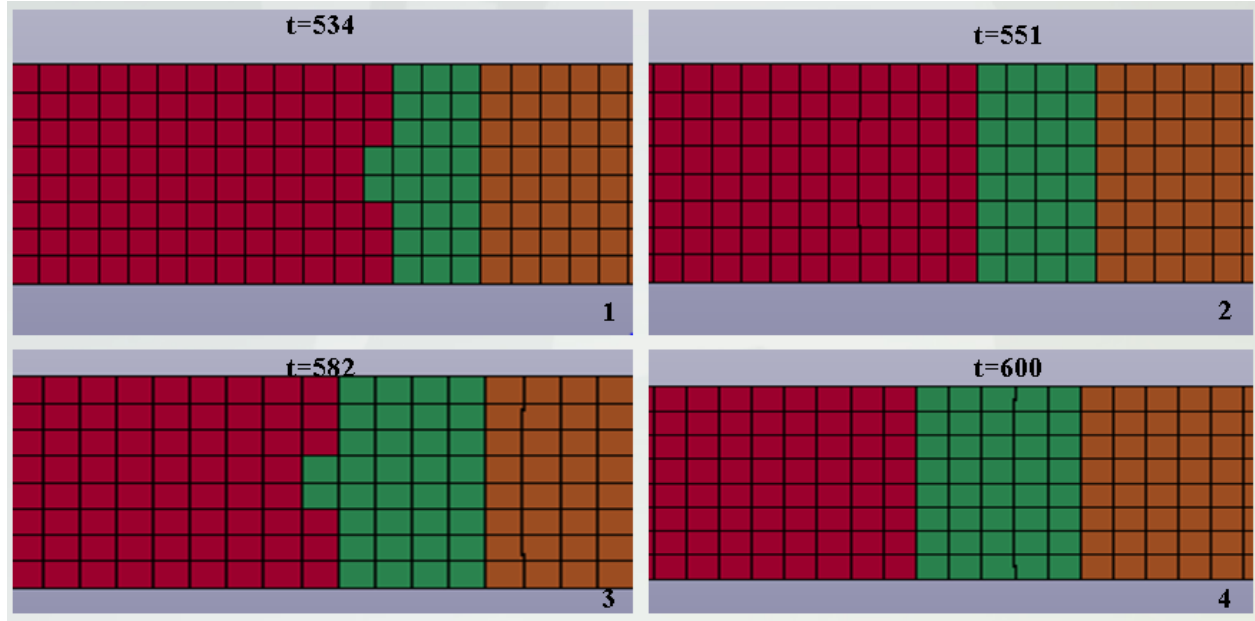


Figure 4.12 Cohesive element deletion of Bilinear CZM

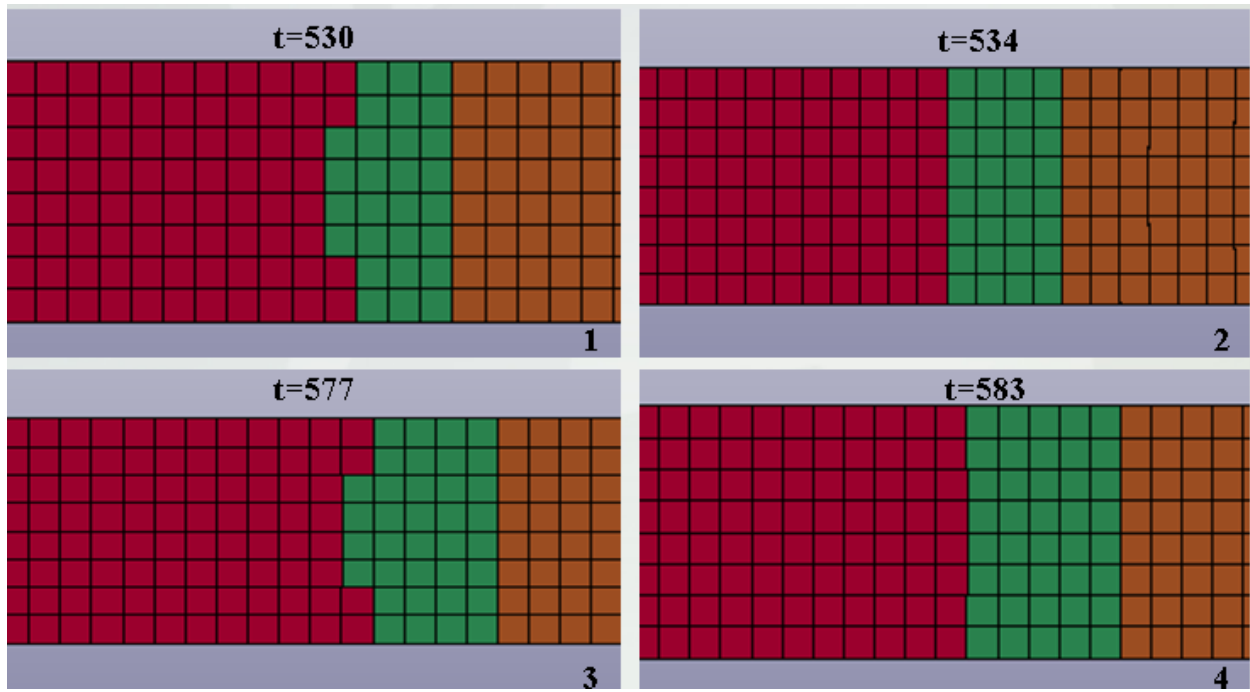


Figure 4.13 Cohesive element deletion of Trilinear CZM

To find out the cause of the instability in Trilinear CZM, the cohesive element deletion in cohesive layer is investigated. Figure 4.12 illustrates the cohesive element deletion inside the cohesive layer for the Bilinear CZM. It takes 17ms for one row of red cohesive elements to be deleted and totally

66ms to delete two rows of cohesive elements. On the contrary, the Trilinear CZM has sudden cohesive element deletion in Figure 4.13. Over the time interval of 4ms, one row of cohesive elements has been deleted because of the element failure. In 53ms, two rows of cohesive elements have been deleted for the Trilinear CZM. The relatively large number of cohesive elements deletion in short amount of time leads to a sudden internal energy transformation which results in instability for Trilinear CZM.

4.1.3 Q3D Composite

The numerical prediction results for the UD composite reveals that the Bilinear CZM is more stable than the Trilinear Cohesive Zone Model in crack propagation. The Bilinear CZM is more viable to simulate Mode I interlaminar fracture toughness test. Higher fracture toughness values are assigned to 60° bias tow cohesive elements which causes several load-drops in load-extension curve. This load-drop phenomenon is also referred as “stick-slip” in literature papers [41-42]. Two

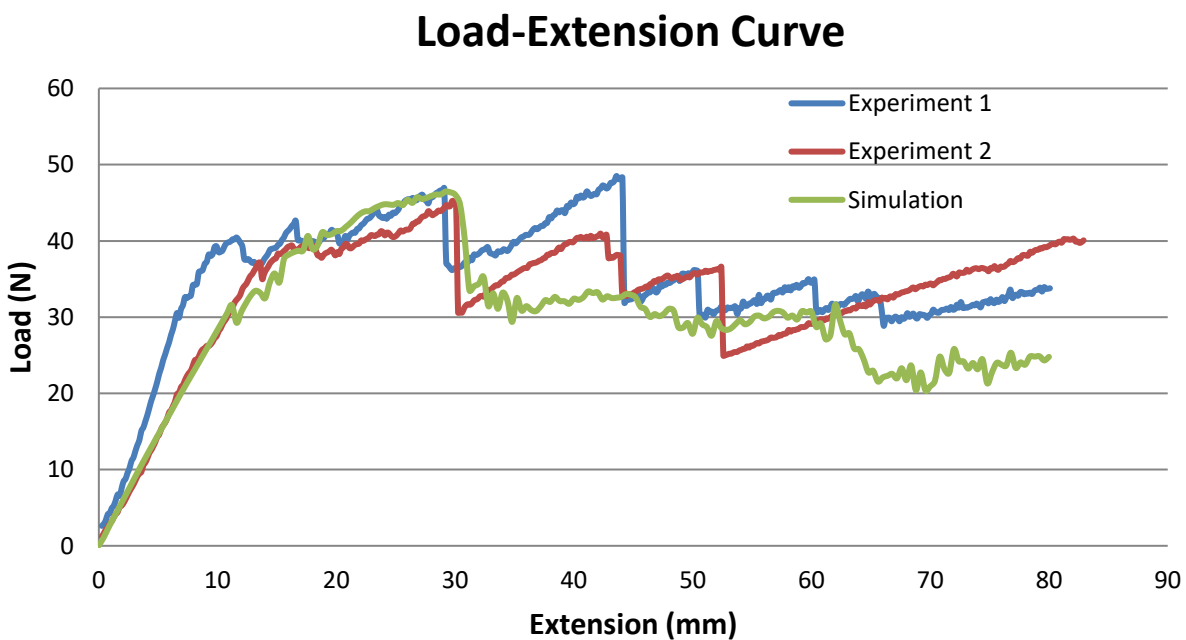


Figure 4.14 Load-Extension curve of Q3D composite laminate with thick cohesive layer

cases for cohesive layer thickness are also investigated here. Looking at numerical prediction of Q3D composite laminate with thick cohesive layer in Figure 4.14, the increase of the elastic load before crack initiation is consistent with the load-extension curve of experiment 2. The numerical prediction of peak load and the first “stick-slip” are agrees well with the experimental result. Each peak in the experimental load-extension curve represents a fiber tow bridging event. Several load drops are observed in the experimental load-extension curve. This phenomenon occurs when a crack starts to propagate and reaches bias bridging tows. As the bias tow has a higher delamination resistance, it requires a higher load to break the fiber tow for crack growth to continue. The general trend of crack growth at the interface agrees with the experimental load-extension curve. However,

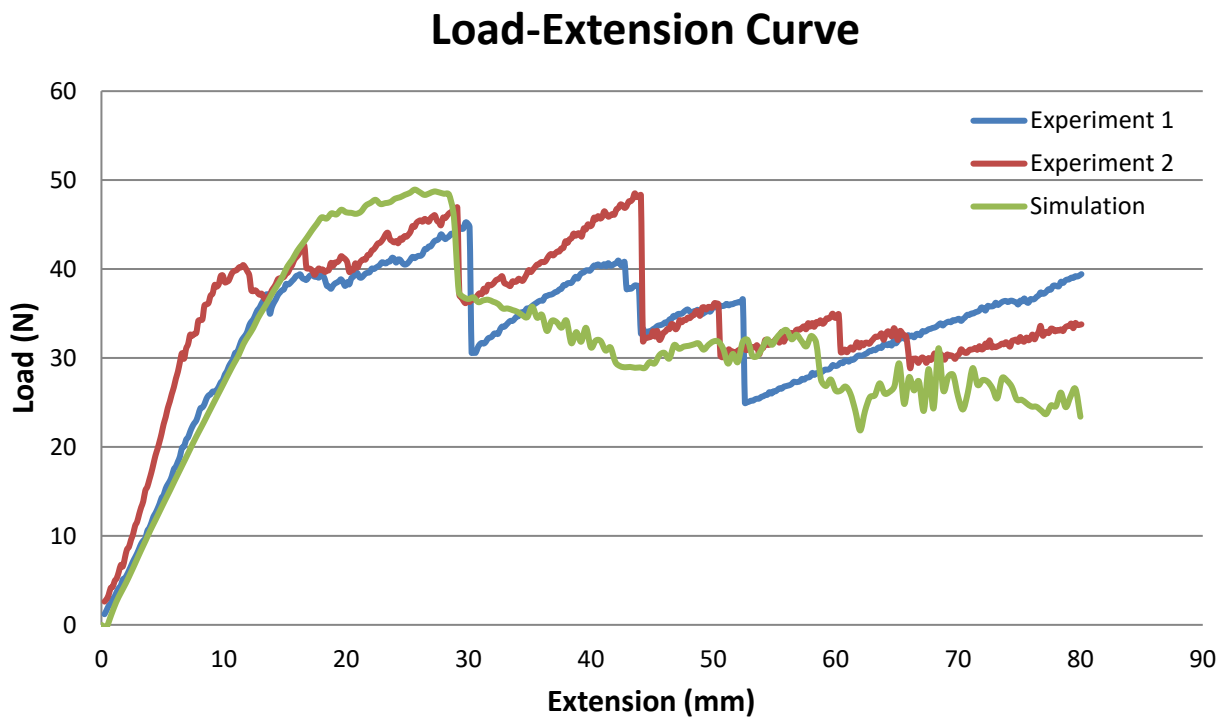


Figure 4.15 Load-Extension curve of Q3D composite laminate with thin cohesive layer

the numerical simulation is not sufficiently accurate to mimic “stick-slip” in the load-extension curve after the peak load.

The load-extension curve of the Q3D composite laminate with thin cohesive layer show consistency of elastic process compared with experiment 2. The peak load is slightly over-predicted. And the “stick-slip” phenomenon is not accurately predicted after the peak load.

4.2 Mode II Results

4.2.1 UD Composite with Bilinear CZM

The numerical prediction of the UD composite with the Bilinear CZM is investigated here. The green curve in Figure 4.16 represents the numerical prediction of bilinear CZM for the UD composite laminate. The elastic part of the load-extension curve before peak load is consistent with experimental results. The model with the Bilinear CZM precisely predict the load to initiate the crack. However, the peak load is under-predicted. The stiffness of the numerical prediction is

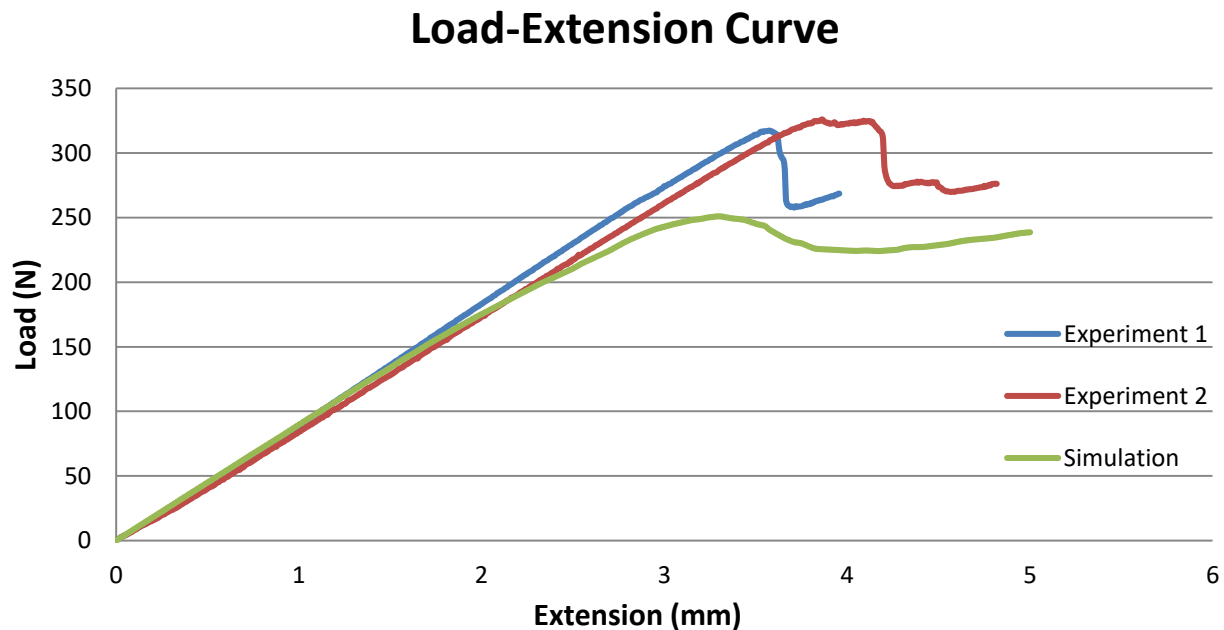


Figure 4.16 Comparison of the ENF experimental Load-deflection curve of UD composite with simulation using the Bilinear CZM.

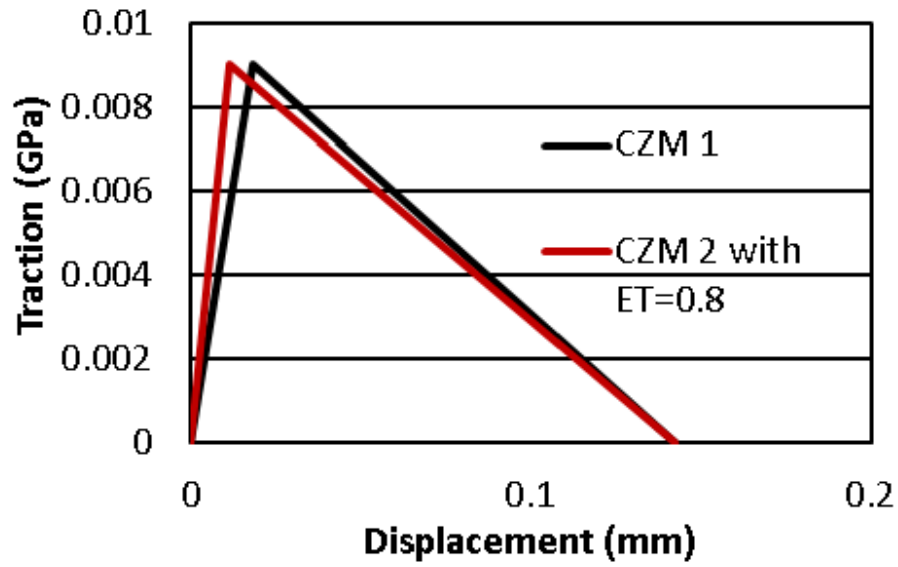


Figure 4.17 CZM comparison with different stiffness

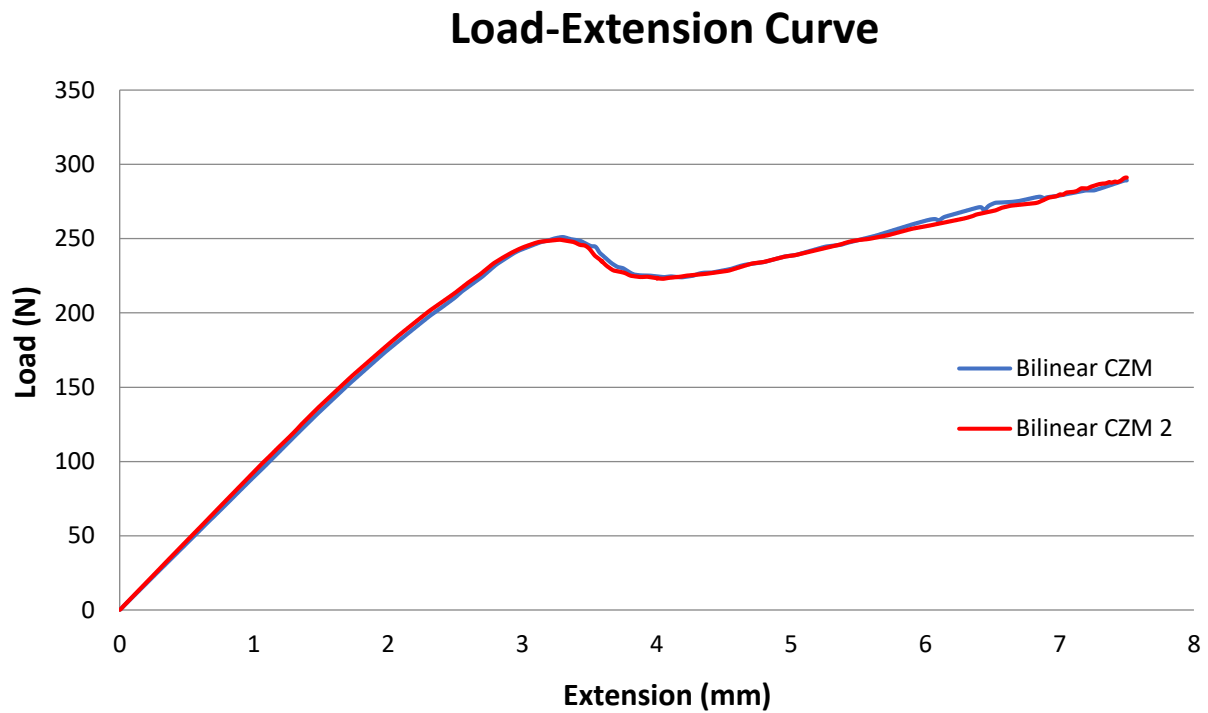


Figure 4.18 Load-deflection curve comparison with two CZMs

reduced because of the crack growth. The sudden load drop after the peak traction of experimental curve does not appear in numerical prediction. To investigate whether the increase of in-plane

stiffness in CZM will stiffen the bending behavior of the composite beams, CZM 2 is introduced with an increased in-plane stiffness (ET). The traction separation curve is presented in Figure 4.17. The stiffness (ET) change results in the shift of the displacement at the peak traction (L). However, the load-extension curves generated in simulations with two CZMs are overlapping each other, Figure 4.18. This shows that the increases of in-plane stiffness (ET) does not affect the numerical prediction results.

4.2.2 UD Composite with Trilinear CZM

Since the Bilinear CZM demonstrates significant stiffness reduction in the elastic part of the load-extension curve and no discrepancy due to load drop after the peak traction, the Trilinear CZM is investigated to see if it can produce different results. The Trilinear CZM result is provided in Figure 4.19. The red and blue curves represent the UD experiment results. The load to initial the

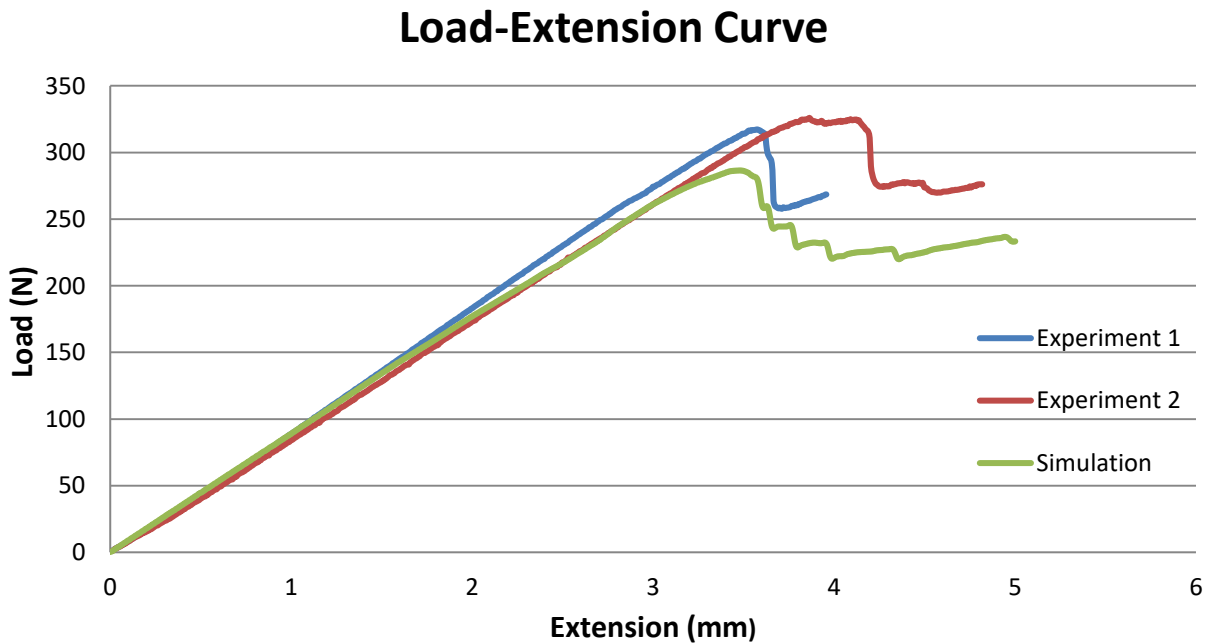


Figure 4.19 Comparison of ENF experimental Load-deflection curve with simulation with a Trilinear CZM.

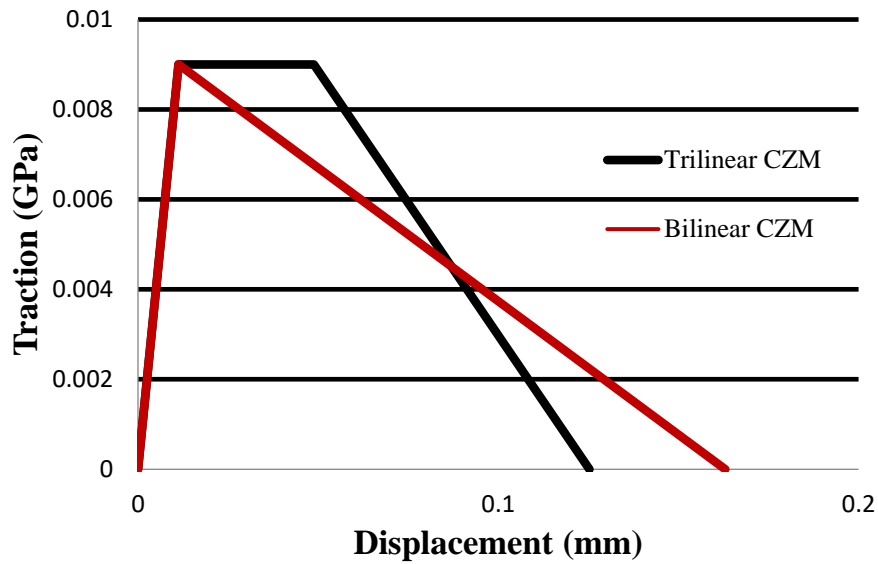


Figure 4.20 Traction-separation curves comparison for Bilinear and Trilinear CZMs

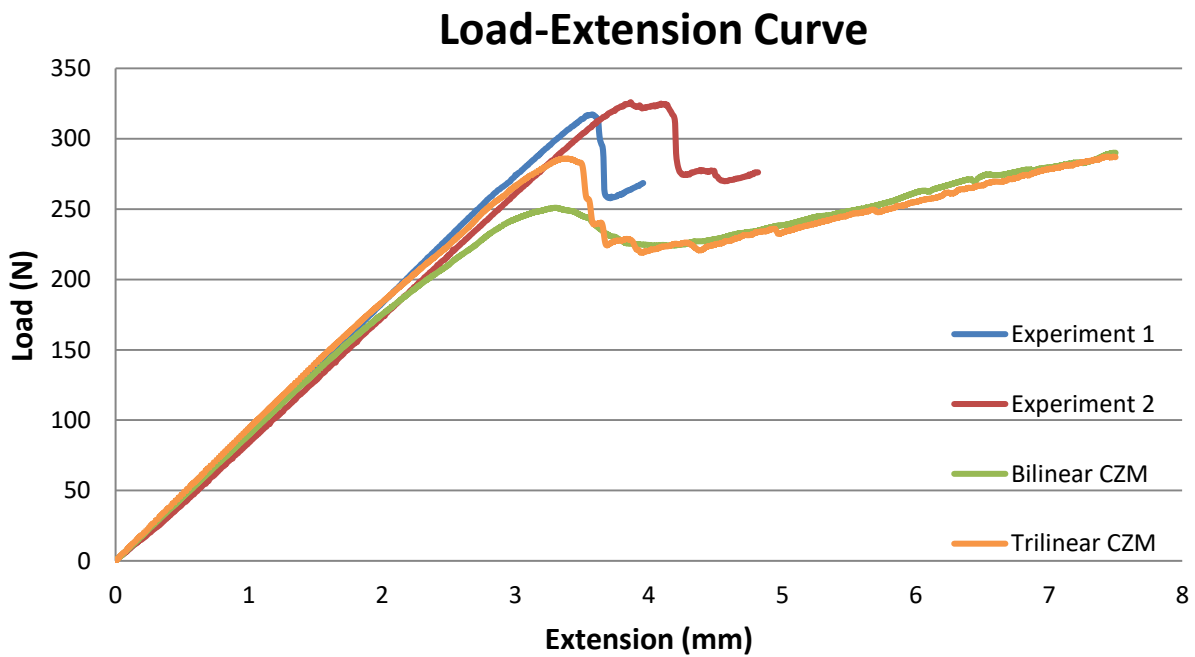


Figure 4.21 Load-extension curves comparison for Bilinear and Trilinear CZMs

crack agrees well with experiment. The decrease of bending stiffness due to crack growth is small compared with the Bilinear CZM. The predicted peak load is slightly smaller than the experimental peak load. The discrepancy after the peak load is observed in Figure 4.19. Instability after the peak

load for Trilinear CZM is also detected in ENF simulation due to sudden cohesive elements deletion. Overall, the Trilinear CZM provides relatively accurate numerical prediction for the delamination behavior of UD composites.

The traction-separation curves for Bilinear and Trilinear CZMs are compared in Figure 4.20, the elastic load increasing to reach the peak traction is the same for both CZMs. The fracture toughness value for both CZMs are the same. The slope of the softening process is steeper for Trilinear CZM.

The load-extension curve in Figure 4.21 shows that the elastic load increase and softening behavior of both CZMs are consistent with each other. The Trilinear CZM predicts a higher peak load for crack to propagates and has less stiffness reduction compared with the Bilinear CZM.

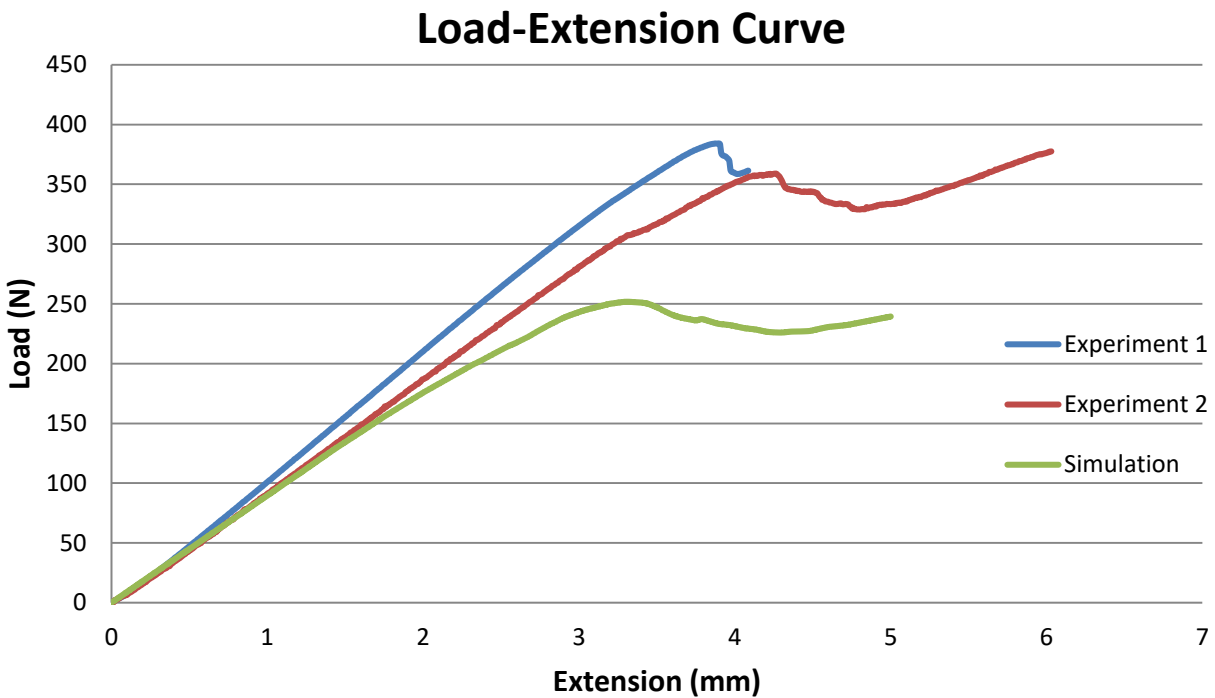


Figure 4.22 Load-extension curve of Bilinear CZM for Mode II

4.2.3 Q3D Composite

Contrary to Mode I DCB test simulations, the model with a Trilinear CZM generated accurate numerical prediction of UD composite under Mode II ENF test. To numerically predict the delamination behavior of Q3D composite, the model with Bilinear CZM was tested first to check the prediction accuracy. Higher fracture toughness values are used for bias tow cohesive elements (brown elements) as shown in Figure 3.4. The load-deflection curve predicted with Bilinear CZM is shown in Figure 4.22. The result revealed an under-prediction of the peak load compared with experimental value (green curve). The Q3D composite became less stiff after the crack starts to propagate. The trend in discrepancy between the experimental curve and predicted response in Q3D ENF simulations with the Bilinear CZM is consistent with UD ENF simulations.

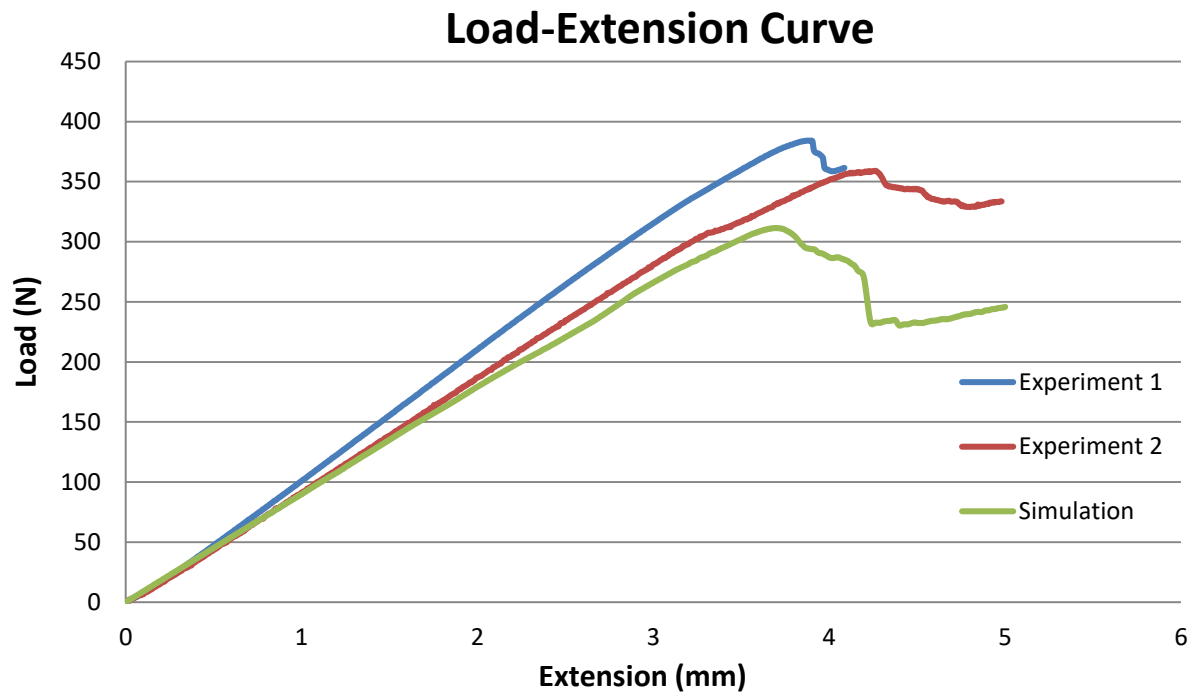


Figure 4.23 Load-extension curve of Trilinear CZM for Mode II

Because the Bilinear CZM failed to accurately predict delamination behavior of Q3D composite laminate, Trilinear CZM was then tested for cohesive layer. A more accurate numerical prediction

is obtained, as shown in Figure 4.23. The bending stiffness reduction is improved compared with Bilinear CZM prediction results in Figure 4.22. The under-prediction of peak load was still seen for Trilinear CZM. The discrepancy of the load drop is more distinct comparing to experimental result. In general, the Trilinear CZM produces more accurate numerical prediction of delamination behavior for Q3D composite laminate than the Bilinear CZM does.

Chapter 5. CONCLUSION

5.1 Summary and Conclusion

In this research, the delamination behavior of UD and Q3D composites are simulated using Cohesive Zone Model (CZM). The interface in UD composite was simulated with one set of CZM parameters. To simulate Q3D composite, two sets of CZM parameters are used. A set of CZM parameter with higher fracture toughness value is assigned to bias tow cohesive elements which have higher delamination resistance. The “stick-slip” behavior of Q3D composites is simulated. Bilinear CZM and Trilinear CZM are used to simulate Mode I and Mode II experiments of UD and Q3D composites. The numerical simulation results of Bilinear CZM and Trilinear CZM are compared with the experimental results, Table 5.1 and 5.2 shows that Bilinear CZM has better accuracy when predicting the peak load of UD and Q3D composites under Mode I condition. The Trilinear CZM gives an unstable softening process of load-extension curve because of sudden cohesive elements deletion in cohesive layer. The load to initiate crack propagation is consistent with experiment. However, numerical simulations could not precisely predict the instability of the crack propagation. The linearity is observed in the elastic part of the load-extension curve.

The two different definitions of shell thickness reference plane result in thick and thin cohesive layer thickness. The results in Table 5.1-5.4 shows that a thick cohesive layer better predicts the peak load and displacement at the peak load for both UD and Q3D composites. To accurately simulate Mode I experiment of UD and Q3D composites, the Bilinear CZM with a thick cohesive layer would be the optimal method. In this thesis, the effect of the fracture toughness value on the numerical simulation results is also investigated, the initial fracture toughness value G_I is used in

Bilinear CZM for the UD composite laminate under Mode I condition. The results show that using the initial fracture toughness value G_I better predicts the load to initiate the crack propagation. On the contrary, using the average fracture toughness value G_{IC} gives a better numerical prediction of crack propagation. A higher fracture toughness value results in a higher peak load of the load-extension curve. The optimal method to numerically predict the delamination behavior of UD composites is to use both G_I and G_{IC} in CZM.

In the Mode II simulation of UD and Q3D composite laminates, both the Bilinear and Trilinear CZMs under-predict the peak load. However, the Trilinear CZM clearly predicts a higher peak load for crack to propagates. The elastic and softening behavior for both CZMs are consistent. Whereas, the stiffness reduction in elastic load increasing process is less for Trilinear CZM. The changing stiffness of CZM does not have significantly influence on simulation results. The instability and discrepancy of the load drop in softening process of load-extension is spotted for Trilinear CZM. In general, Table 5.1-5.4 show that the Trilinear CZM, when simulating UD and Q3D composites under Mode I and Mode II conditions, demonstrates a better prediction accuracy of the peak load and displacement at the peak load compared with Bilinear CZM.

Table 5.1 Comparison of the predicted and measured peak load with Bilinear CZM

	Mode I with Bilinear CZM				Mode II with Bilinear CZM	
	UD (Thick)	UD (Thin)	Q3D (Thick)	Q3D (Thin)	UD	Q3D
Predicted peak load (N)	49.3	51.6	46.5	48.38	251	252
Measured peak load (N)	46.598	46.598	45.23	45.23	317.25	358.9
Error (%)	5.5	9.7	2.7	6.5	-26.4	-42.4

Table 5.2 Comparison of the predicted and measured peak load with Trilinear CZM

	Mode I with Trilinear CZM		Mode II with Trilinear CZM	
	UD (Thick)	UD (Thin)	UD	Q3D
Predicted peak load (N)	52	52.7	287	311
Measured peak load (N)	46.598	46.598	317.25	358.9
Error (%)	10.4	11.6	-10.5	-15.4

Table 5.3 Comparison of the predicted and measured displacement at the peak load with Bilinear CZM

	Mode I with Bilinear CZM				Mode II with Bilinear CZM	
	UD (Thick)	UD (Thin)	Q3D (Thick)	Q3D (Thin)	UD	Q3D
Predicted displacement at peak load (mm)	13.44	13.2	29.2	28.4	3.32	3.35
Measured displacement at peak load (mm)	19.41	19.41	29.75	29.75	3.57	4.27
Error (%)	-44.4	-47.0	-1.9	-4.8	-7.5	-27.5

Table 5.4 Comparison of the predicted and measured displacement at the peak load with Trilinear CZM

	Mode I with Trilinear CZM		Mode II with Trilinear CZM	
	UD (Thick)	UD (Thin)	UD	Q3D
Predicted displacement at peak load (mm)	14.2	14	3.49	3.74
Measured displacement at peak load (mm)	19.41	19.41	3.57	4.27
Error (%)	-36.7	-38.6	-2.3	-14.2

5.2 Future Work

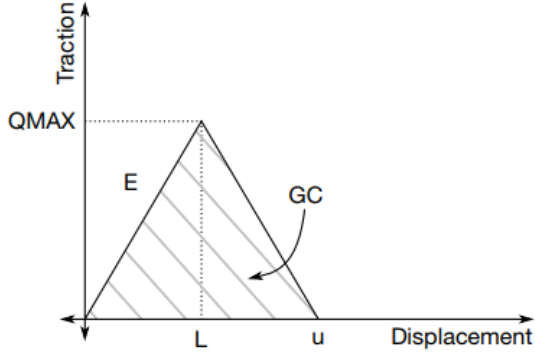
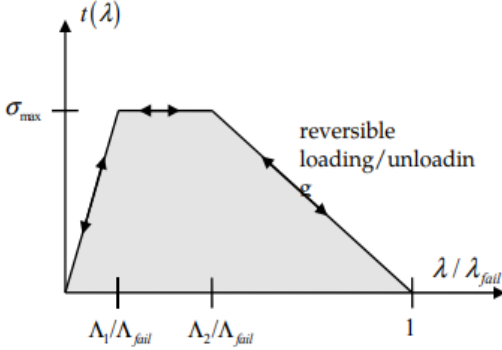
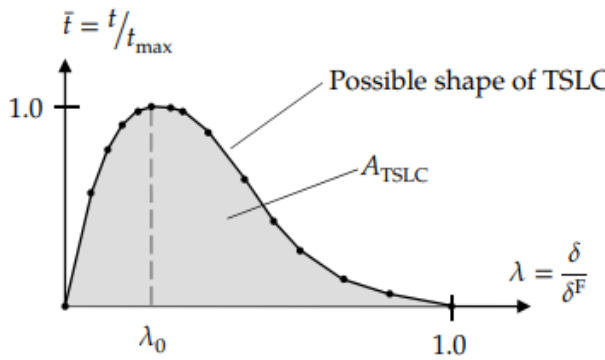
To further improve the numerical model, the following works are suggested: (1) validate the numerical model by simulating Mode III and mixed-mode fracture toughness test, and (2) examine the numerical model by simulating impact test.

In addition, a systematic characterization of the mechanical properties of Q3D composite is recommended. This would give accurate input of composite properties in LS-DYNA which could improve the numerical prediction accuracy on softening process of load-extension curve.

Accurately identifying the fiber bridging area at the interface of Q3D composite laminates using microscope could also improve the accuracy of prediction on softening process of load-extension curve. In the Mode II simulation of Q3D composites, the instability of softening process is observed for Trilinear CZM. Other cohesive zone law could implement in cohesive zone model such as arbitrary normalized traction-separation law. Instead of having discontinuities of traction-separation law for Bilinear and Trilinear CZMs [43], arbitrary normalized traction-separation law is continuous throughout the curve which might reduce the instability of the softening process.

APPENDIX

Table A.1 Different Cohesive Zone Laws

MAT_138	
MAT_185	
MAT_186	
MAT_041_050	<p>User defined material model, toughness and peak can be defined with different values</p>

BIBLIOGRAPHY

BIBLIOGRAPHY

- [1] Rosario, Kirit, and Dahsin Liu. "Assessment of Quasi-Three-Dimensional Composites - with Discussions on Fiber Straining and Weaving Effectiveness." *Journal of Composite Materials*, vol. 44, no. 25, Dec. 2010, pp. 2953–2973.
- [2] A.P. Mouritz, Compression properties of z-pinned composite laminates, *Composites Science and Technology*, Volume 67, Issues 15–16, 2007, Pages 3110-3120, ISSN 0266-3538, <https://doi.org/10.1016/j.compscitech.2007.04.017>.
- [3] Dickinson LC, Farley GL, Hinders MK. Prediction of effective three-dimensional elastic constants of translaminar reinforced composites. *J Comp Materials* 1999; 33:1002–29.
- [4] Grassi, M & Zhang, Xiang & Meo, Michele. (2002). Prediction of stiffness and stresses in z-fibre reinforced composite laminates. *Composites Part A: Applied Science and Manufacturing*. 33. 1653-1664. 10.1016/S1359-835X (02)00137-9.
- [5] Tan, K. T., Watanabe, N., Sano, M., Iwahori, Y., & Hoshi, H. (2010). Interlaminar Fracture Toughness of Vectran-stitched Composites - Experimental and Computational Analysis. *Journal of Composite Materials*, 44(26), 3203–3229. <https://doi.org/10.1177/0021998310369581>
- [6] Tony Wentz, Xinyu Mao, Danielle Zeng, Jeff Dahl, Xinran Xiao, Interlaminar fracture toughness of a quasi 3D braided composite, ASC conference paper, 2019
- [7] W. Zhou, Peridynamic modeling and impact testing of dynamic damage, fracture, and failure process in fiber-reinforced composite materials. PhD thesis, Michigan State University, 2018.
- [8] A.B. Nair, R. Joseph, Eco-friendly bio-composites using natural rubber (NR) matrices and natural fiber reinforcements, Editor(s): Shinzo Kohjiya, Yuko Ikeda, *Chemistry, Manufacture and Applications of Natural Rubber*, Woodhead Publishing, 2014, Pages 249-283, ISBN 9780857096838.
- [9] H Mao, S Mahadevan, Fatigue damage modelling of composite materials, *Composite Structures*, Volume 58, Issue 4, 2002, Pages 405-410, ISSN 0263-8223.

- [10] Philippe H Geubelle, Jeffrey S Baylor, Impact-induced delamination of composites: a 2D simulation, *Composites Part B: Engineering*, Volume 29, Issue 5, 1998, Pages 589-602, ISSN 1359-8368.
- [11] Rosario, Kirit & Liu, Dahsin. (2010). Assessment of Quasi-Three-Dimensional Composites - with Discussions on Fiber Straining and Weaving Effectiveness. *Journal of Composite Materials - J COMPOS MATER.* 44. 2953-2973.
- [12] Tabiei, Ala, and Wenlong Zhang. "14th International LS-DYNA Conference." *A Robust Cohesive Zone Model for Cyclic Loading*.
- [13] Dominik Bender, Jens Schuster, Dirk Heider, Flow rate control during vacuum-assisted resin transfer molding (VARTM) processing, *Composites Science and Technology*, Volume 66, Issue 13, 2006, Pages 2265-2271, ISSN 0266-3538.
- [14] Roberts, Gary, D.; Goldberg, Robert, K.; Binienda, Wieslaw, K.; Arnold, William, A.; Littell, Justin, D.; Kohlman, Lee, W. "Characterization of Triaxial Braided Composite Material Properties for Impact Simulation", NASA, 2009.
- [15] Liu Sheng, Quasi-impact damage initiation and growth of thick-section and toughened composite materials, *International Journal of Solids and Structures*, Volume 31, Issue 22, 1994, Pages 3079-3098, ISSN 0020-7683, [https://doi.org/10.1016/0020-7683\(94\)90042-6](https://doi.org/10.1016/0020-7683(94)90042-6).
- [16] Zou, Z., Reid, S. R., Li, S., & Soden, P. D. (2002). Modelling Interlaminar and Intralaminar Damage in Filament-Wound Pipes under Quasi-Static Indentation. *Journal of Composite Materials*, 36(4), 477–499. <https://doi.org/10.1177/0021998302036004539>.
- [17] Krueger, R., 2002. "The virtual crack closure technique: history, approach and applications". NASA/CR-2002-211628, ICASE Report No. 2002-10, April 2012.
- [18] E.F. Rybicki, M.F. Kanninen, A finite element calculation of stress intensity factors by a modified crack closure integral, *Engineering Fracture Mechanics*, Volume 9, Issue 4, 1977, Pages 931-938, ISSN 0013-7944, [https://doi.org/10.1016/0013-7944\(77\)90013-3](https://doi.org/10.1016/0013-7944(77)90013-3).
- [19] I.S. Raju, Calculation of strain-energy release rates with higher order and singular finite elements, *Engineering Fracture Mechanics*, Volume 28, Issue 3, 1987, Pages 251-274, ISSN 0013-7944, [https://doi.org/10.1016/0013-7944\(87\)90220-7](https://doi.org/10.1016/0013-7944(87)90220-7).

- [20] Viggo Tvergaard, John W. Hutchinson, The relation between crack growth resistance and fracture process parameters in elastic-plastic solids, *Journal of the Mechanics and Physics of Solids*, Volume 40, Issue 6, 1992, Pages 1377-1397, ISSN 0022-5096.
- [21] Needleman AA. A Continuum Model for Void Nucleation by Inclusion Debonding. *ASME. J. Appl. Mech.* 1987;54(3):525-531. doi:10.1115/1.3173064.
- [22] G.T. Camacho, M. Ortiz, Computational modelling of impact damage in brittle materials, *International Journal of Solids and Structures*, Volume 33, Issues 20–22, 1996, Pages 2899-2938, ISSN 0020-7683, [https://doi.org/10.1016/0020-7683\(95\)00255-3](https://doi.org/10.1016/0020-7683(95)00255-3).
- [23] Ku-Hyun Jung, Do-Hyoung Kim, Hee-June Kim, Seong-Hyun Park, Kyung-Young Jhang, Hak-Sung Kim, Finite element analysis of a low-velocity impact test for glass fiber-reinforced polypropylene composites considering mixed-mode interlaminar fracture toughness, *Composite Structures*, Volume 160, 2017, Pages 446-456, ISSN 0263-8223.
- [24] A. Matzenmiller, J. Lubliner, R. Taylor. A constitutive model for anisotropic damage in fiber-composites *Mech Mater*, 20 (1995), pp. 125-152.
- [25] LS-DYNA Keyword User's Manual, Volume II, Material Models, 2018.
- [26] D. M. Liljedahl, C & D. Crocombe, A & Abdel Wahab, Magd & Ashcroft, Ian. (2006). Damage modelling of adhesively bonded joints. *International Journal of Fracture*. 141. 147-161. 10.1007/s10704-006-0072-9.
- [27] A. Turon, P.P. Camanho, J. Costa, J. Renart, Accurate simulation of delamination growth under mixed-mode loading using cohesive elements: Definition of interlaminar strengths and elastic stiffness, *Composite Structures*, Volume 92, Issue 8, 2010, Pages 1857-1864, ISSN 0263-8223, <https://doi.org/10.1016/j.compstruct.2010.01.012>.
- [28] Camanho, P. P., et al. "Numerical Simulation of Mixed-Mode Progressive Delamination in Composite Materials." *Journal of Composite Materials*, vol. 37, no. 16, Aug. 2003, pp. 1415–1438.
- [29] Seung J. Song and Anthony M. Waas. "Energy-based mechanical model for mixed mode failure of laminated composites", *AIAA Journal*, Vol. 33, No. 4 (1995), pp. 739-745. <https://doi.org/10.2514/3.12639>.

- [30] Xie, De, et al. "Discrete Cohesive Zone Model to Simulate Static Fracture in 2D Triaxially Braided Carbon Fiber Composites." *Journal of Composite Materials*, vol. 40, no. 22, Nov. 2006, pp. 2025–2046, doi:10.1177/0021998306061320.
- [31] A.P. Mouritz, Review of z-pinned composite laminates, *Composites Part A: Applied Science and Manufacturing*, Volume 38, Issue 12, 2007, Pages 2383-2397, ISSN 1359-835X, <https://doi.org/10.1016/j.compositesa.2007.08.016>.
- [32] Cox, B & Narayanaswamy, Sridhar. (2002). A Traction Law for Inclined Fiber Tows Bridging Mixed-Mode Cracks. *Mechanics of Advanced Materials and Structures*. 9. 299-331. 10.1080/15376490290096973.
- [33] Chen, Leishan & G. Ifju, Peter & Sankar, Bhavani. (2005). Analysis of Mode I and Mode II Tests for Composites with Translaminar Reinforcements. *Journal of Composite Materials - J COMPOS MATER*. 39. 1311-1333. 10.1177/0021998305050425.
- [34] ASTM D5528 Standard test method for mode I interlaminar fracture toughness of unidirectional fiber-reinforced polymer matrix composites. In: *Annual book of ASTM standards* vol. 15.06. USA: ASTM;2002.
- [35] ASTM, "Standard Test Method for Determination of the Mode II Interlaminar Fracture Toughness of Unidirectional Fiber-Reinforced Polymer Matrix Composites," in *ASTM D7905/D7905M-14*, ed. West Conshohocken, PA: ASTM International 2014.
- [36] "Contact Types." Welcome to the LS-DYNA Support Site, www.dynasupport.com/tutorial/contact-modeling-in-ls-dyna/contact-types.
- [37] LS-DYNA Keyword User's Manual, Volume I, LS-DYNA R7.1, May 26, 2014.
- [38] Saha, C., et al. "Processing and Performance Evaluation of Hollow Microspheres Filled Epoxy Composites."
- [39] Gareth W. Beckermann, Kim L. Pickering, Mode I and Mode II interlaminar fracture toughness of composite laminates interleaved with electrospun nanofibre veils, *Composites Part A: Applied Science and Manufacturing*, Volume 72, 2015, Pages 11-21, ISSN 1359-835X.

- [40] I.S. Floros, K.I. Tserpes, T. Löbel, Mode-I, mode-II and mixed-mode I+II fracture behavior of composite bonded joints: Experimental characterization and numerical simulation, *Composites Part B: Engineering*, Volume 78, 2015, Pages 459-468, ISSN 1359-8368.
- [41] Yasuyo Tanzawa, Naoyuki Watanabe, Takashi Ishikawa, Interlaminar fracture toughness of 3-D orthogonal interlocked fabric composites, *Composites Science and Technology*, Volume 59, Issue 8, 1999, Pages 1261-1270, [https://doi.org/10.1016/S0266-3538\(98\)00167-5](https://doi.org/10.1016/S0266-3538(98)00167-5).
- [42] Kimberley A. Dransfield, Laut K. Jain, Yiu-Wing Mai, On the effects of stitching in CFRPs—I. mode I delamination toughness, *Composites Science and Technology*, Volume 58, Issue 6, 1998, Pages 815-827, ISSN 0266-3538, [https://doi.org/10.1016/S0266-3538\(97\)00229-7](https://doi.org/10.1016/S0266-3538(97)00229-7).
- [43] A. Turon, P.P. Camanho, J. Costa, C.G. Dávila, A damage model for the simulation of delamination in advanced composites under variable-mode loading, *Mechanics of Materials*, Volume 38, Issue 11, 2006, Pages 1072-1089, ISSN 0167-6636, <https://doi.org/10.1016/j.mechmat.2005.10.003>.